Gastroenterology 2019;157:1279–1292

Metabolic Functions of Gut Microbes Associate With Efficacy of Tumor Necrosis Factor Antagonists in Patients With Inflammatory Bowel Diseases

Konrad Aden,[1,2,*] **Ateequr Rehman**,[1,*] **Silvio Waschina**,[3,*] Wei-Hung Pan,[1] Alesia Walker,[4] Marianna Lucio,[4] Alejandro Mena Nunez,[1] Richa Bharti,[1] Johannes Zimmerman,[3] Johannes Bethge,[2] Berenice Schulte,[2] Dominik Schulte,[2] Andre Franke,[1] Susanna Nikolaus,[2] Johann Oltmann Schroeder,[2] Doris Vandeputte,[5] Jeroen Raes,[5] Silke Szymczak,[6] Georg H. Waetzig,[7] Rainald Zeuner,[2] Philippe Schmitt-Kopplin,[4] Christoph Kaleta,[3,§] Stefan Schreiber,[1,2,§] and Philip Rosenstiel[1,§]

[1]Institute of Clinical Molecular Biology, Christian-Albrechts-University and University Hospital Schleswig-Holstein, Campus Kiel, Kiel, Germany; [2]Department of Internal Medicine I., Christian-Albrechts-University and University Hospital Schleswig-Holstein, Campus Kiel, Kiel, Germany; [3]Institute for Experimental Medicine, Christian-Albrechts-University and University Hospital Schleswig-Holstein, Campus Kiel, Kiel, Germany; [4]Research Unit Analytical BioGeoChemistry, Helmholtz ZentrumMünchen, German Research Centre for Environmental Health (GmbH), Neuherberg, Germany; [5]VIB-KU Leuven Center for Microbiology, Campus Gasthuisberg, Leuven, Belgium; [6]Institute of Medical Informatics and Statistics, University of Kiel, Kiel, Germany; and [7]CONARIS Research Institute AG, Kiel, Germany

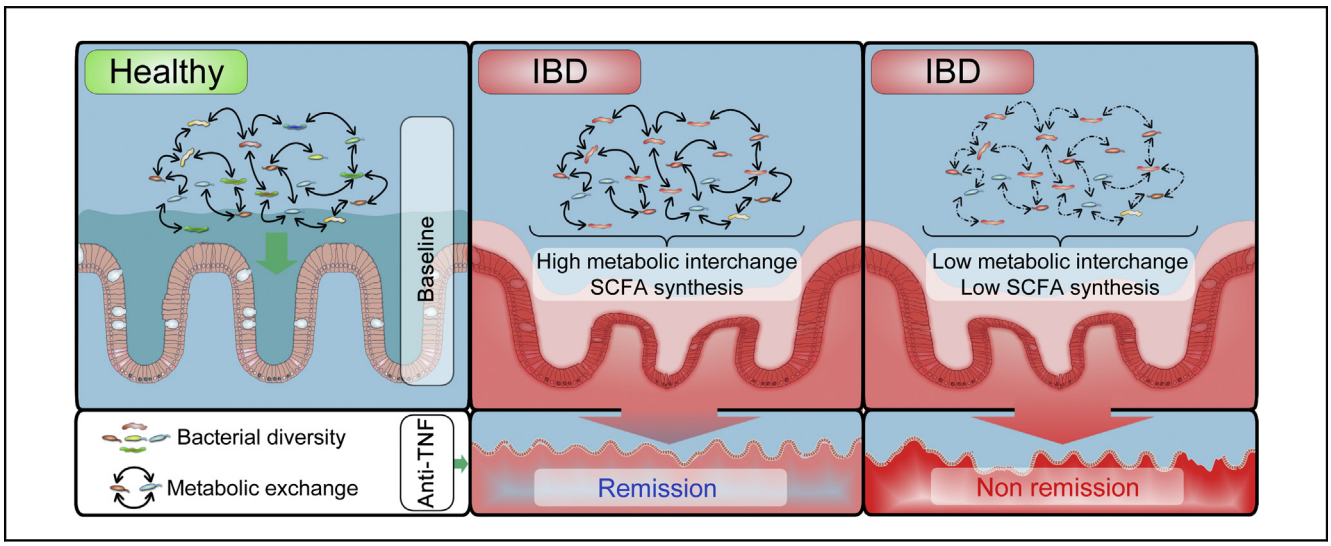

See Covering the Cover synopsis on page 1175.

BACKGROUND & AIMS: Altered interactions between the mucosal immune system and intestinal microbiota contribute to pathogenesis of inflammatory bowel diseases (IBD). It is not clear how inhibitors of cytokines, such as antagonists of tumor necrosis factor (anti-TNF), affect the intestinal microbiome. We investigated the effects of anti-TNF agents on gut microbe community structure and function in a longitudinal 2-step study of patients with IBD. We correlated our findings with outcomes of treatment and investigated patterns of metabolites in fecal samples before and after anti-TNF therapy. **METHODS:** We performed a prospective study of 2 cohorts of patients in Germany; the discovery cohort comprised 12 patients with IBD, 17 patients with rheumatic disease, and 19 healthy individuals (controls); fecal samples were collected at baseline and 2, 6, and 30 weeks after induction of anti-TNF therapy. The validation cohort comprised 23 patients with IBD treated with anti-TNF or vedolizumab (anti-$\alpha4\beta7$ integrin) and 99 healthy controls; fecal samples were collected at baseline and at weeks 2, 6, and 14. Fecal microbiota were analyzed by V3–V4 16S ribosomal RNA gene amplicon sequencing. Clinical response and remission were determined by clinical disease activity scores. Metabolic network reconstruction and associated fecal metabolite level inference was performed in silico using the AGORA (Assembly of Gut Organisms through Reconstruction and Analysis) resource. Metabolomic analyses of fecal samples from a subset of patients were performed to validate metabolites associated with treatment outcomes. **RESULTS:** Anti-TNF therapy shifted the diversity of fecal microbiota in patients with IBD, but not with rheumatic disease, toward that of controls.

Across timepoints, diversity indices did not vary significantly between patients with IBD who did or did not achieve clinical remission after therapy. In contrast, in silico modeling of metabolic interactions between gut microbes found metabolite exchange to be significantly reduced at baseline in fecal samples from patients with IBD and to be associated with later clinical remission. Predicted levels of butyrate and substrates involved in butyrate synthesis (ethanol or acetaldehyde) were significantly associated with clinical remission following anti-TNF therapy, verified by fecal metabolomic analyses. **CONCLUSIONS:** Metabolic network reconstruction and assessment of metabolic profiles of fecal samples might be used to identify patients with IBD likely to achieve clinical remission following anti-TNF therapy and increase our understanding of the heterogeneity of IBD.

Keywords: Crohn's Disease; Ulcerative Colitis; Inflammation; Short-Chain Fatty Acid.

WHAT YOU NEED TO KNOW

BACKGROUND & CONTEXT

TNF antagonists represent a current mainstay in IBD therapy, but therapeutic efficacy is hampered by primary and secondary loss of response. The intestinal microbiome has been suggested to be implicated into to host immune response to biologic therapy. Whether gut microbial functions contribute to anti-TNF efficacy in IBD is not known.

FINDINGS

Anti-TNF therapy shifted the diversity of fecal microbiota in patients with IBD toward that of healthy individuals. Levels of butyrate and substrates involved in butyrate synthesis were significantly associated with clinical remission following anti-TNF therapy.

LIMITATIONS

Further investigations in larger longitudinal IBD cohorts are necessary to delineate in detail the associations of gut microbial metabolic signatures with therapy outcome in IBD.

IMPACT

In silico modelling of metabolic profiles of fecal samples might be used to identify patients with IBD likely to achieve remission following anti-TNF therapy. These analyses might also provide information about the pathogenesis of IBD.

Inflammatory bowel disease (IBD), with its main entities Crohn's disease (CD) and ulcerative colitis (UC), can be considered an archetypal disease entity of a larger, heterogeneous group of chronic inflammatory diseases (CIDs), characterized by a dysbalanced immune system, leading to excessive proinflammatory cytokine production and destructive local inflammation.[1,2] CIDs affect different organs through their primary manifestation but are characterized by common systemic immune perturbations. The underlying etiology comprises a polygenic susceptibility with more than 200 risk variants and loci identified for IBD until today[3–5] and many of these are shared among the different CID entities. Shared disease genes are preferentially involved in the regulation of innate and adaptive immune responses and are thought to affect the homeostasis of host-microbiota interactions.[6,7] Intestinal dysbiosis has been detected across CIDs.[8,9] Although dysbiosis in IBD[10–13] is likely influenced by immune dysregulation and destruction of the epithelial interface by local inflammation, the etiology of dysbiosis seen in other CIDs without overt inflammation in the gut is still vague and comprises shifts of specific bacterial taxonomical groups and enrichment of potentially harmful taxa; for example *Eggerthella lenta* in rheumatoid arthritis (RA).[14,15] Despite an immanent need to understand the underlying mechanism of dysbiosis, a systematic comparison of gut microbial communities in intestinal vs nonintestinal-driven inflammatory disease is missing so far. Blockade of tumor necrosis factor (TNF) has evolved as a therapeutic principle that is effective across different CIDs.[16,17] Although the use of anti-TNF antibodies is a mainstay for the therapy in CID, the development of antibodies directed against other proinflammatory cytokines (interleukin-6, interleukin-1β) and lately also the exploitation of other principles (e.g., blockade of integrin-mediated immune cell trafficking in IBD),[18] has led to an increased complexity in the treatment of these CID entities.

To what extent targeted therapies are able to interfere with altered gut microbial community structures and metabolic function is unknown. Likewise, whereas it was shown in cancer therapy that efficacy of targeted therapies, such as immunotherapy as well as classical chemotherapy, is critically modulated by gut microbial community composition,[19,20] it is unknown whether gut microbiota and related metabolic properties are associated with therapeutic outcome. Here, we investigated the role of anti-TNF therapy on longitudinal dynamics of gut microbial composition and metabolic function in a 2-tiered approach. First, we investigated the influence of anti-TNF on gut microbial diversity by 16S ribosomal RNA (rRNA) phylogenetic profiling and ecosystem-scale metabolic modeling in patients with IBD or rheumatic diseases. We show that inferred microbial metabolic interactions are associated with response to anti-TNF therapy in patients with IBD. In a second step, we validated our findings in an independent IBD cohort and found that microbial metabolite interactions are able to discriminate between anti-TNF remitter and nonremitters. Using in silico prediction of metabolite exchange and stool metabolomics,

* Authors share co-first authorship; § Authors share co-senior authorship.

Abbreviations used in this paper: **AGORA, Assembly of Gut Organisms through Reconstruction and Analysis; BASDAI, Bath Ankylosing Spondylitis Disease Activity Index; CD, Crohn's disease; CID, chronic inflammatory disease; HBI, Harvey-Bradshaw Index for CD; HC, healthy control; IBD, inflammatory bowel disease; PERMANOVA, permutational multivariate analysis of variance; RA, rheumatoid arthritis; rRNA, ribosomal RNA; SCFA, short-chain fatty acid; TNF, tumor necrosis factor; UC, ulcerative colitis.**

Most current article

0016-5085
https://doi.org/10.1053/j.gastro.2019.07.025

we show that, among other principles, butyrate levels are significantly altered between patients achieving remission vs nonremitting patients. We thereby demonstrate that (1) 16S rRNA based functional prediction of metabolic cooperativity might serve as a novel approach for predicting clinical response to TNF antagonists in patients with IBD, and (2) identify the short-chain fatty acid (SCFA) butyrate as a clinical marker for therapeutic efficacy in IBD.

Materials and Methods

Patient Recruitment and Study Design

Human study subjects were recruited at the outpatient clinic of the University Hospital Schleswig-Holstein, Campus Kiel, to obtain fecal samples. Treatment decisions were made due to clinical requirements after discussion at the interdisciplinary inflammatory medicine board of the hospital. The design of the prospective studies had no influence on treatment or other clinical actions. Patients were naïve to biological treatment or had at least paused prior biologic therapy for more than 12 weeks. The study was approved by the ethics committee of the Christian-Albrechts-University of Kiel (A 124/14 and AZ 156/03–2/13) and subjects provided written informed consent.

For the discovery cohort (cohort 1), patients were recruited from 2 major patient groups: (1) 12 patients with intestinal inflammation (ie, IBD, UC [n = 4], CD [n = 8]), or (2) with non-IBD rheumatic diseases (ie, seropositive RA [n = 10], seronegative RA [n = 2], ankylosing spondylitis [n = 5]), which are collectively termed rheumatic diseases (n = 17) hereafter. Patients were asked to collect morning feces before (24 hours) and at designated time points (2, 6, and 30 weeks) after anti-TNF therapy initiation. Fecal samples were collected using feces collection tubes with prefilled DNA stabilizer (Stratec, Birkenfeld, Germany) and stored at −80°C until further use. Anti-TNF agents comprised infliximab, certolizumab pegol, adalimumab, and etanercept. Single time-point samples from a group of 19 healthy, untreated subjects were included at the same time and using identical sampling procedures were included into the study as controls. For the validation cohort (cohort 2), a total of 23 biologics-naïve patients with IBD (CD = 10, UC = 13) were recruited, who received first-time anti-TNF (infliximab, n = 10) or anti-$\alpha4\beta7$ integrin antibody (vedolizumab, n = 13) therapy. Patients were investigated within a 24-hour time frame before initiation of treatment and at weeks 2, 6, and 14 after initiation of treatment, including collection of morning feces. Single time-point fecal 16S rRNA gene microbial profiles from a cross-sectional cohort of healthy individuals (n = 99) sampled in the time frame of the study served as a reference map to assess the directionality of microbial changes after anti-TNF therapy initiation for cohort 2. Overview of patient characteristics are detailed in Supplementary Table 1. Overview of clinical efficacy data for the 2 cohorts is shown in Supplementary Tables 2 and 3, respectively. A detailed overview about cohort composition and molecular analyses is given in Supplementary Figure 1.

Patient Assessment

All patients were scheduled for biologic therapy for medical reasons and received drug at least until week 22. Clinical disease indices were assessed at baseline and at weeks 2, 6, 14, and 30 after therapy initiation using clinical disease scores (Disease Activity Score 28 for RA [DAS28], Bath Ankylosing Spondylitis Disease Activity Index [BASDAI], Harvey-Bradshaw Index for CD [HBI], or Mayo score for UC).[21] In RA, clinical response was defined as a reduction of the DAS28 score by more than 1.2 points, whereas clinical remission was defined as a DAS28 <2.6. For ankylosing spondylitis, the BASDAI clinical response was defined as a reduction of 50% (BASDAI50) at week 6, whereas clinical remission was defined as a BASDAI <4. Responders in the HBI for CD were defined by a decrease of ≥2 points in HBI, whereas nonresponders showed a decrease of <2 points or an increase in HBI. Patients with CD with an HBI of ≤4 were considered to be in remission, and those with ≥5 to have active disease. In patients with UC, a decrease of the partial Mayo score of ≥2 points and ≥30% with either a decrease of rectal bleeding ≥1 or with rectal bleeding ≤1 were defined as responders. Patients with a partial Mayo score of ≤2 (bleeding 0) were considered to be in remission, and those with ≥3 to have active disease. Histopathological scoring of biopsies was performed by standard clinical procedures in a blinded fashion by a trained pathologist, and the overall grade of inflammation was grouped according to normal (0), mild (1), moderate (2), or severe inflammation (3), and the respective values were used for pathology score calculation.

Statistical Analyses

Phylotype abundances were subsampled to the lowest number of sequences within the analyzed sample and relative abundances were $\log_{10}$-normalized. Principal coordinate analysis was performed on abundance (Bray-Curtis) and presence/absence (Jaccard) based distance matrices. One-way permutational multivariate analysis of variance (PERMANOVA) was performed to test the statistical significance of microbial community differences in healthy subjects and patients with IBD or rheumatic diseases. Both principal coordinate analysis and PERMANOVA were performed in PAST software and principle coordinates were visualized in the vegan package v.2.0–10 in R software V 3.0.3 (https://cran.r-project.org/web/packages/vegan/index.html). We employed the Θ_{YC} (Yue-Clayton) similarity index[22] to measure the shift of microbiota before and after initiation of treatments (within and between disease groups) as well as directionality in reference to healthy subject microbiota. This similarity index is based on the species abundance of shared as well as nonshared species applying even weighting to all species in communities. The nonparametric Mann-Whitney *U* test was used to test the significance of diversity/distance differences between healthy subjects and patients (IBD/rheumatic diseases) at different time points. The nonparametric Wilcoxon matched-pairs signed rank test was used to observe the significance of changes before and after therapy initiation within a disease group. Indicator species analysis[23] was performed to identify indicator bacterial phylotypes between healthy control (HC) group and patients (IBD and rheumatic diseases) before and 30 weeks after therapy initiation. This approach takes relative abundance and relative frequency of occurrence in 2 sets of samples[24] into account.

Microbial Community Modeling

We used reconstructed metabolic models of 773 human gut bacterial species[25] (AGORA [Assembly of Gut Organisms

through Reconstruction and Analysis] resource) to predict metabolic potential and biochemical interactions between bacterial species. We extensively refined the originally published models to remove erroneous futile cycles that occurred in community simulations and often caused unreasonably high exchange fluxes between bacteria (see Supplementary Table 6 for details). By mapping 16S rRNA sequences to the corresponding models contained in AGORA and combining them to a community-level metabolic model, we derived patient-specific models of the respective microbial community. Using these models, we inferred ecological relationships (mutualism, competition, antagonism) and potential metabolite exchange interactions with the host. Please refer to the Supplementary Materials and Methods for a more detailed description.

Results

CIDs Are Characterized by Intestinal Dysbiosis

We investigated microbiota community structures of IBD, healthy controls (HC) and patients with rheumatic diseases (seropositive/seronegative RA or ankylosing spondylitis) at baseline. This discovery cohort comprised longitudinal fecal samples of a total of 29 patients (IBD = 12, rheumatic diseases = 17) before and after anti-TNF therapy initiation and single time-point fecal samples from HC (n = 19) (Supplementary Tables 1 and 2); 16S rRNA gene sequencing of all samples (including baseline and post therapeutic intervention) resulted in the identification of 388 phylotypes (Supplementary Table 4, Supplementary Materials and Methods). As all statistical algorithms assessing $\alpha-$diversity have inherent strengths and weaknesses, we used a set of $\alpha-$diversity indices, including (1) observed and (2) estimated (Chao I) richness, (3) evenness of species considering abundance (nonparametric Shannon), and (4) phylogenetic distance (phylodiversity score). Comparing all groups, baseline microbial communities between HCs and the rheumatic disease or IBD groups, respectively, were significantly different, as shown by nonparametric Kruskal-Wallis test. To interrogate pairwise baseline differences of microbial α-diversity between specific groups, we used the Mann-Whitney *U* test, which, for the pair IBD vs HC, showed significantly reduced $\alpha-$diversity index values for (1) observed ($P = 0.024$; Figure 1*A*) and (2) estimated (Chao I) richness ($P = 0.019$; Figure 1*B*), (3) NP Shannon index of diversity ($P = 0.0001$; Figure 1*C*), and (4) phylogenetic diversity ($P = 0.017$; Figure 1*D*). Patients with rheumatic diseases also had reduced bacterial diversity compared with HC, but the index levels were only significant for the NP Shannon diversity index (Figure 1*C*). Principal coordinate analysis on membership- (Jaccard) and abundance-based (Bray-Curtis) $\beta-$diversity distance matrices demonstrate that the first 2 coordinates were able to separate samples for a health/disease descriptor status. PERMANOVA test on Jaccard (Figure 1*E*) distances showed a significantly distinct microbial composition among IBD, rheumatic diseases, and HC. Similarly, abundance (Bray-Curtis)-based analysis revealed significant differences in patients with IBD and rheumatic diseases compared with HC, but the differences were not significant between rheumatic diseases and IBD communities (Figure 1*F*). These observations confirm earlier findings[11] showing that the baseline intestinal microbial communities of patients with IBD are characterized by a reduced number of species and diminished richness and evenness ($\alpha-$diversity) as well as altered community composition and structure ($\beta-$diversity). In contrast, intestinal microbiota from patients with rheumatic diseases only display shifts in community structure ($\beta-$diversity) compared with HC, indicating a disease effect on the gut microbiota even in the absence of overt intestinal inflammation.

Effects of Anti-TNF Treatment on Microbial Diversity in IBD and Rheumatic Diseases Are Reflected on the β- But Not α-diversity Level

To analyze the effect of anti-TNF treatment on intestinal microbiota in IBD (n = 12) and rheumatic diseases (n = 17) independently, we assessed α-diversity indices before and 2, 6, and 30 weeks after first-time anti-TNF therapy induction and used the samples of the HC group as a reference point. The observed and estimated species richness and phylodiversity in patients with IBD increased after the beginning of therapeutic intervention and reached statistical significance at week 30 compared with baseline. This shift was directed toward the controls, and the distance between diversities of treatment-naïve IBD fecal samples and HCs became nonsignificant after 30 weeks of therapy (Figure 2*A–D*). Similar differences were not observed for the NP Shannon diversity index (Figure 2*C*). In contrast, restoration of bacterial diversities was not evident in patients with rheumatic diseases (Figure 2*E–H*). Interestingly, we failed to identify a discrimination between remitting and nonremitting patients based on α-diversity restorations (Supplementary Figure 2), which could also be due to limited sample size. We next investigated β-diversity indices to measure longitudinal community composition changes before and after therapy initiation. We assessed the interindividual dissimilarity using Yue and Clayton distance matrix, which considers not only membership overlap, but also species abundance between communities.[22] Pairwise comparison of distances between samples at baseline and during treatment (2, 6, and 30 weeks) showed increased interindividual dissimilarity among anti-TNF–treated IBD patients (Supplementary Figure 3*A*). This indicates that anti-TNF treatment induces an increase of heterogeneity of the intestinal microbiota between patients with IBD. In contrast to IBD, anti-TNF treatment in patients with rheumatic diseases during treatment was associated with an overall decrease of dissimilarity (week 30 vs pretreatment) of the microbiota (Supplementary Figure 3*B*). This indicates an overall constriction of microbial β-diversity (ie, a gain of similarity) among patients with rheumatic diseases. To understand the directionality of the observed changes, we compared dissimilarity between healthy subjects and disease groups (IBD, rheumatic diseases) before and during therapeutic intervention and observed that anti-TNF treatment shifted the microbial communities of both patient groups toward healthy subjects, indicating a subtle corrective effect of

anti-TNF treatment on microbial dysbiosis of both disease entities, IBD and rheumatic diseases (Supplementary Figure 3*C* and *D*). Again, a discrimination between clinical remission and nonremission was not observable (data not shown).

Individual Phylotype Alterations After Anti-TNF Treatment

We next determined indicator bacterial phylotypes that were significantly different between HC and anti-TNF–treated patients with IBD or rheumatic diseases at baseline and asked whether these taxa would alter their abundance on anti-TNF treatment (week 30). In IBD, we identified 14 indicator phylotypes that were significantly different between HC from untreated IBD (Supplementary Table 5). On anti-TNF treatment, all 14 identified phylotypes lost the indicator species status, suggesting that these phylotypes are normalized on anti-TNF treatment (Figure 3*A*). In IBD, *Coprococcus* (indicator value, 84.37; $P = .003$) and *Roseburia inulinivorans* (indicator value, 79.25; $P = .031$) were the top indicator phylotypes at baseline (based on *P* value, compared with HC). Both indicator phylotypes displayed reduced abundance compared with healthy subjects at week 0 and increased their abundance over the time course of treatment, leading to loss of significance between HC and IBD at week 30 (Figure 3*B*, Supplementary Table 5). In patients with rheumatic diseases, we identified 5 indicator phylotypes, which, by abundance, were significantly different between baseline and HC and lost the indicator status after anti-TNF treatment at week 30 (Supplementary Figure 4*A*, Supplementary Table 6). Of those 5 indicator taxa, the abundance of the top indicator phylotypes (week 0 compared with HC, based on *P* value) Erysipelotrichaceae (indicator value, 81.33; $P = .009$) and *Dorea* (indicator value, 68.81; $P = .042$) increased significantly to become nonindicators in posttreatment samples at week 30 (Supplementary Figure 4*B*). Strikingly, none of these identified taxa were significantly associated with therapeutic outcome of anti-TNF treatment (remission/nonremission). We therefore hypothesized that such outcome-associated shifts might be better visible in the inferred metabolic pathways and functional properties of the microbiota, which are known to display a greater interindividual consistency compared with the highly variable abundance of individual taxa.[26]

Stabilizing Ecological Interactions Are Less Frequent in IBD and Rheumatic Diseases

As diversity measurements and individual taxa identification in our exploratory cohort were not able to predict therapy outcome in IBD, we next used in silico metabolic modeling from 16S rRNA sequencing data to infer metabolic interactions within the luminal microbiota and associated fecal metabolite levels. We hypothesized that metabolic functions rather than taxonomical composition might affect response to TNF antagonists. For this purpose, we used the recently published AGORA resource, a comprehensive assembly of metagenomics data from 773 human gut bacterial species, designed to predict metabolic interactions among microbial communities based on 16S rRNA data.[25] We categorized ecological relationships between 2 different bacterial organisms into mutualistic interactions, antagonistic interactions, and resource competition, depending on the benefit that the individual partners obtained from the predicted interactions. Although mutualistic and antagonistic interactions can increase community dynamics,[27,28] interspecific resource competition can reduce community stability.[27] Interestingly, the predicted frequencies for mutualistic pairwise interactions did not show significant differences between patients with IBD or rheumatic diseases compared with HCs. However, we found that in IBD, and to a lesser degree in rheumatic diseases, the predicted frequency of antagonistic interactions was significantly reduced at the beginning of the therapy and partially restored toward the end of the treatment (Figure 4*A*). Vice versa, we observed an enhanced interspecific resource competition of gut bacteria in both inflammatory diseases, indicating a reduced stability of microbial communities.

Metabolic Cross-feeding Is Impaired in Patients With IBD and Rheumatic Diseases and Associated With Lack of Clinical Efficacy of Anti-TNF Therapy

To evaluate whether anti-TNF treatment also affects the rates (or fluxes) of metabolite exchange between organisms (referred to as "metabolic interchange"), we used metabolic network modeling to predict the exchange of metabolites between bacterial community members in the individual samples using in silico microbial community models (for details see Supplementary Materials and Methods). The simulation results indicated that nonremitting patients with IBD or rheumatic diseases, compared with HCs, displayed a baseline reduction of total metabolic interchange, which also remained below the levels of HC after 30 weeks of anti-TNF treatment (Figure 4*B*). This was in contrast to patients achieving clinical remission, who did not display a reduction of the predicted metabolic interchange (Figure 4*B*) compared with HCs. These data point toward different microbial metabolic signatures that might affect therapeutic efficacy and contribute to clinical remission. In summary, the in silico modeling of the gastrointestinal bacterial metabolism indicated a strong disruption of ecosystem functioning within IBD and rheumatic diseases gut microbiomes, which was partly restored upon anti-TNF therapy.

Anti-TNF Therapy Restores Disrupted Gut Microbial Community Metabolism in IBD

We next aimed to validate our central hypothesis that impaired metabolic cross-feeding is associated with clinical outcome of anti-TNF therapy in IBD using a second, independent longitudinal IBD cohort (see Supplementary Table 7). In this context, we also aimed to investigate whether these potential effects were attributed to anti-TNF therapy alone or reflected a generalizable effect of successful remission induced by treatment with biologics. We

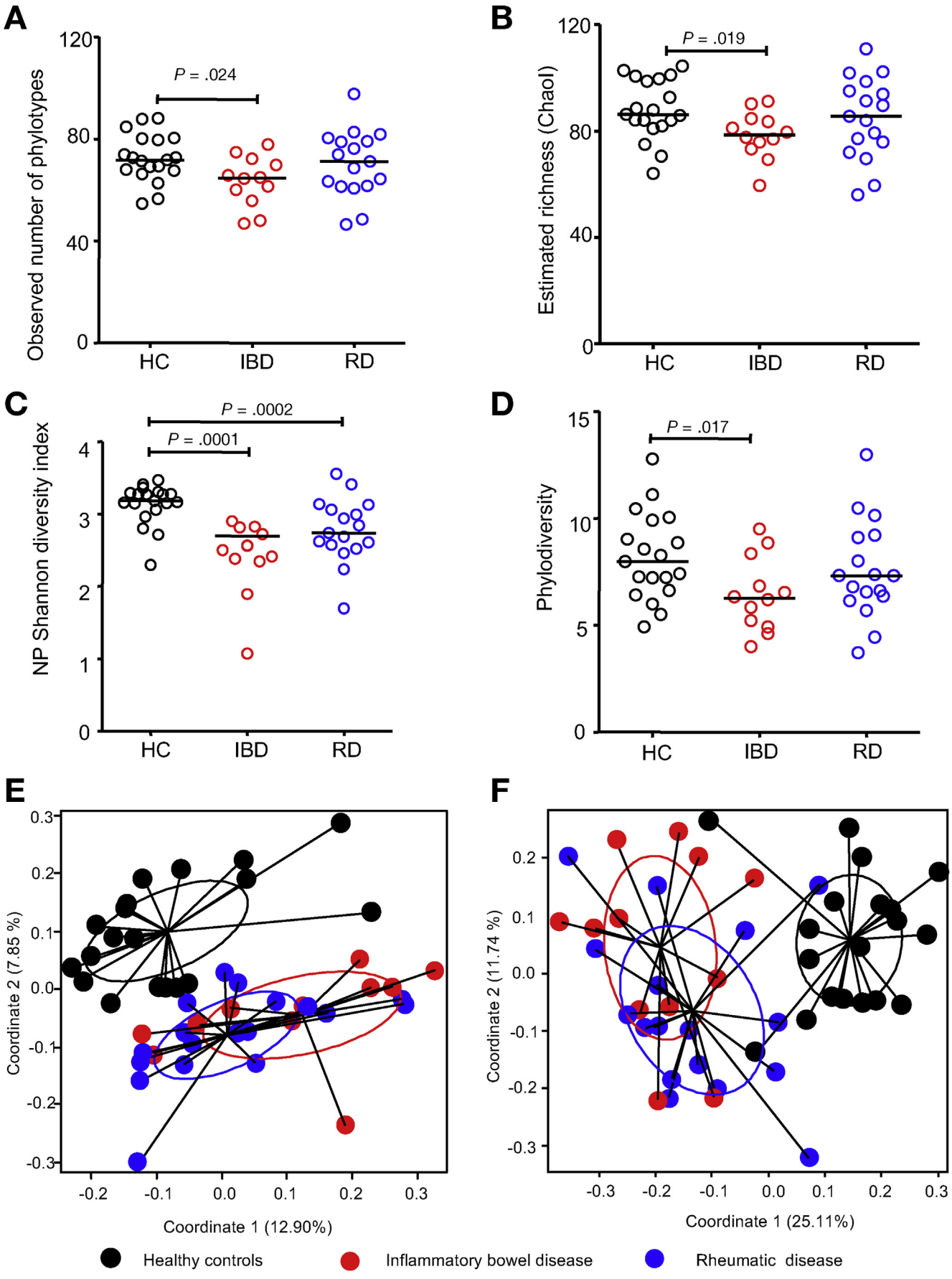
A
Observed number of phylotypes
120
80
40
0
P = .024
HC
IBD
RD
B
Estimated richness (Chao1)
120
80
40
0
P = .019
HC
IBD
RD
C
NP Shannon diversity index
4
3
2
1
0
P = .0002
P = .0001
HC
IBD
RD
D
Phylodiversity
15
10
5
0
P = .017
HC
IBD
RD
E
Coordinate 2 (7.85 %)
0.3
0.2
0.1
0.0
-0.1
-0.2
-0.3
-0.2
-0.1
0.0
0.1
0.2
0.3
Coordinate 1 (12.90%)
F
Coordinate 2 (11.74 %)
0.2
0.1
0.0
-0.1
-0.2
-0.3
-0.3
-0.2
-0.1
0.0
0.1
0.2
0.3
Coordinate 1 (25.11%)
Healthy controls
Inflammatory bowel disease
Rheumatic disease

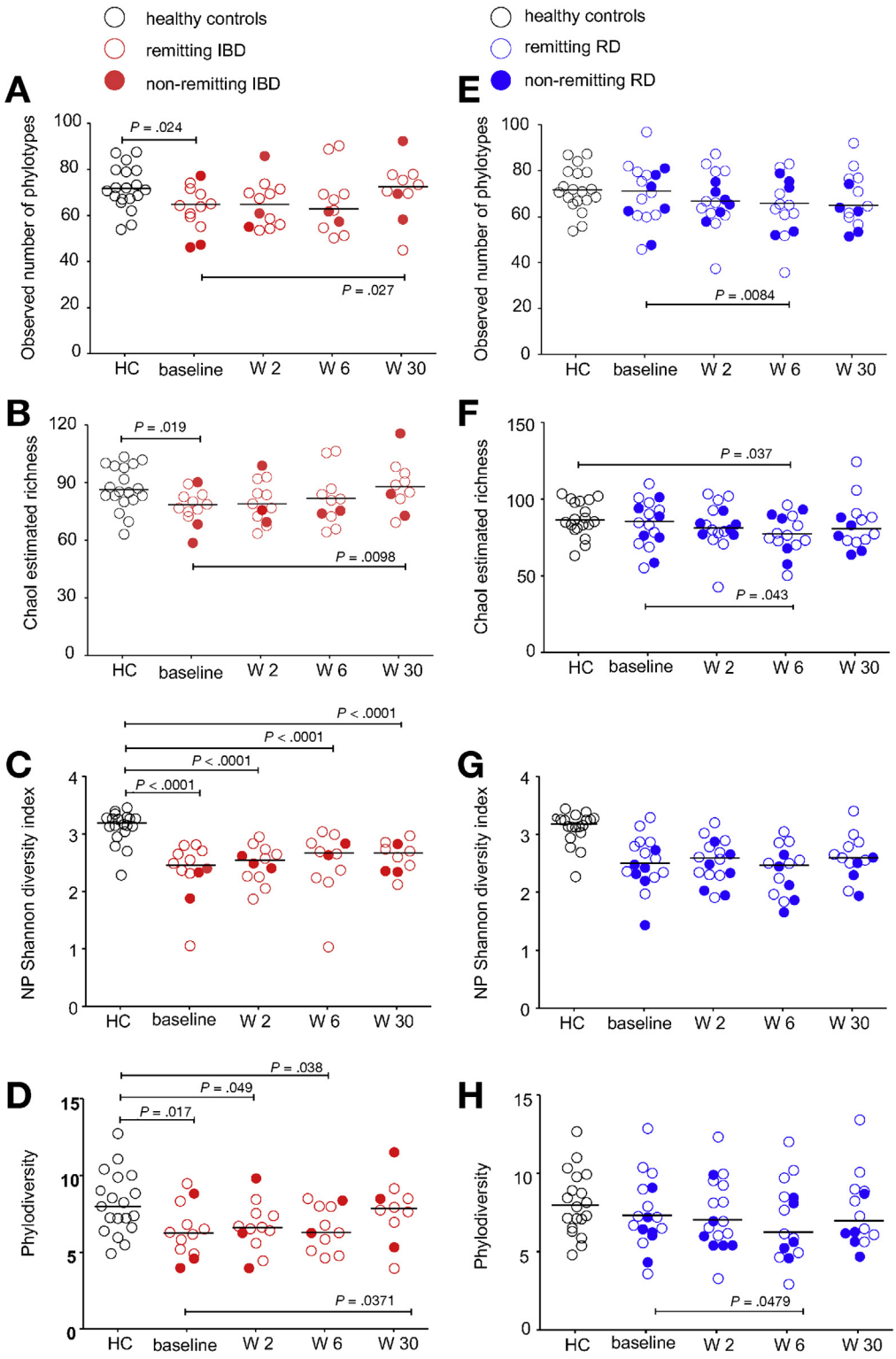

Figure 2. Anti-TNF therapeutic intervention restores α-diversity in IBD, but not in rheumatic diseases (RD). Observed number of phylotypes (*A* and *E*), estimated species richness (*B* and *F*), NP Shannon diversity (*C* and *G*) and phylodiversity (*D* and *H*) indices were assessed in fecal samples collected from patients with IBD or RD at baseline and after initiation of anti-TNF interventions (W, week). HCs served as benchmark for normal microbial diversities. Remitters are shown as open circles, whereas non-remitters are shown as filled circles. Significance of observed differences were determined by Wilcoxon matched-pairs signed rank test (pairwise comparison: before and after the beginning of therapeutic interventions) or Mann-Whitney *U* test (HCs compared with patients).

Figure 1. α- and β-diversity of intestinal microbial communities in IBD, rheumatic diseases (RD), and HCs. α-diversity indices as estimated by observed number of phylotypes (*A*), estimated richness (*B*), NP Shannon index of diversity (*C*) and phylodiversity (*D*). Principal coordinate plots based on Jaccard (*E*) and Bray-Curtis (*F*) distances. Significance of differences in α-diversity indices were determined by the Mann-Whitney *U* test. Significance of differences in β-diversity was assessed by PERMANOVA statistics. Bonferroni-corrected *P* values: Bray-Curtis: (HC–IBD, $P = .0003$; HC–RD, $P = .0003$; IBD–RD, $P = .0366$); Jaccard (HC–IBD, $P = .0003$; HC–RD, $P = .0003$; IBD–RD, $P = .237$).

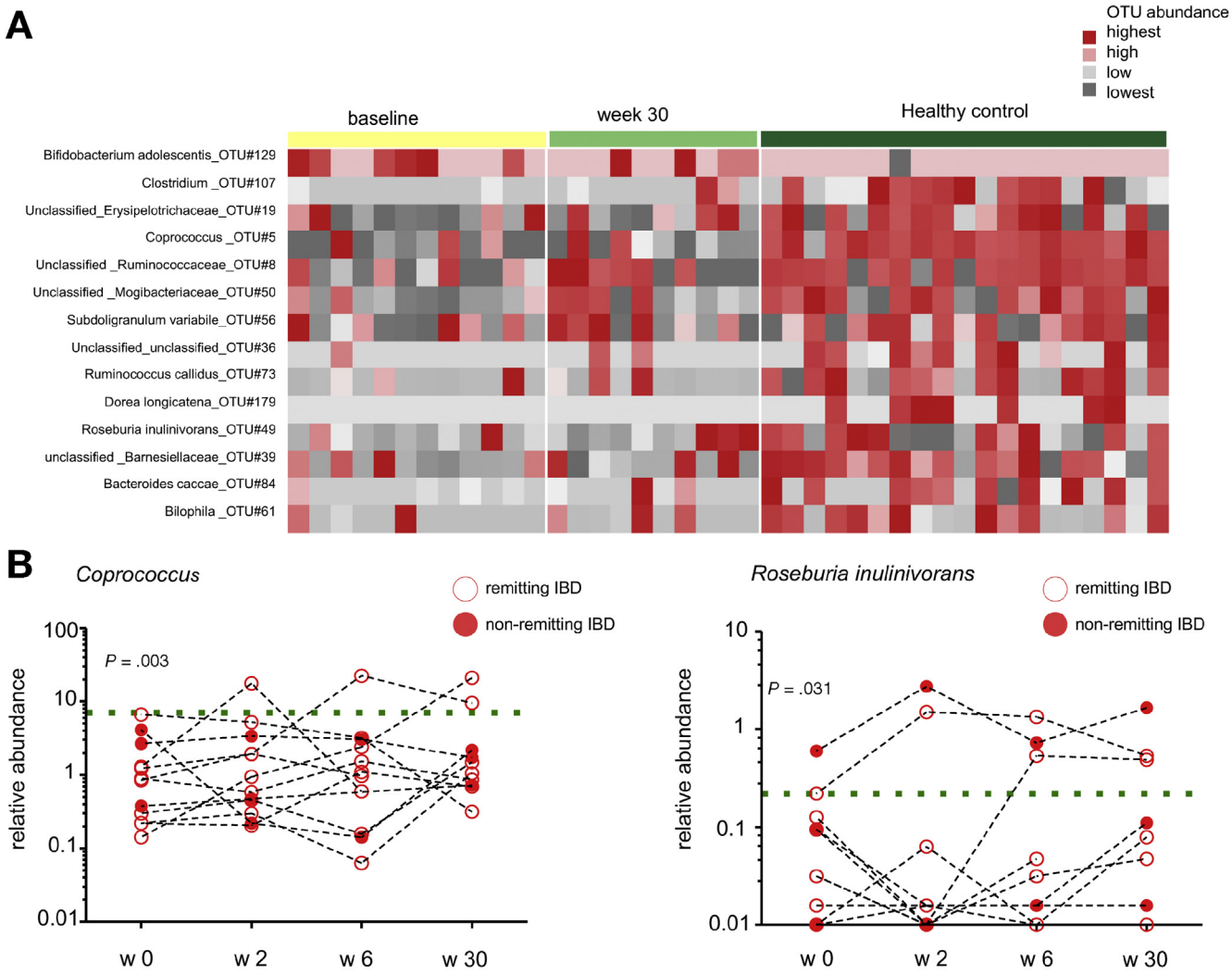

Figure 3. Anti-TNF intervention partly restores phylotype alterations in IBD. (*A*) Loss (down) or gain (up) of indicator species status was determined in relation to HC group microbiota. Relative abundance signal values were transformed into Z-scores for visualization. Each column represents an individual patient, whereas each row represents the relative abundance of labeled indicator species. (*B*) Representative indicator phylotypes that were significantly decreased at week 0 compared with HCs and increased in abundance after anti-TNF therapeutic intervention to become comparable to HC subject status (median = green dashed line) at week 30. *P* values indicate the statistical significance at week 0 between patients with IBD and HCs.

recruited a total of 23 patients (CD = 10, UC = 13) (cohort 2), who underwent first-time therapy with either anti-TNF (infliximab) or anti-$\alpha4\beta7$ integrin (vedolizumab) antibodies and collected fecal samples at baseline and at weeks 2, 6, and 14 after therapy induction (Supplementary Table 3). To exclude a priori differences on the dietary intake that might influence microbial community structure, we assessed the dietary intake in a subgroup of patients (n = 7 patients, anti-TNF treatment; n = 3 remitting, n = 4 nonremitting) using the validated Potsdam Dietary Questionnaire[29] and were not able to observe significant differences in the intake of carbohydrates, fibers, protein, or fat between patients achieving remission or nonremitting patients (data not shown). However, a thorough assessment is needed to fully understand effects of dietary intake on the predicted metabolic properties of the gut microbiota. We performed metabolic cross-feeding analysis on the 16S data sets from the longitudinal fecal samples of either anti-TNF– or anti-$\alpha4\beta7$-integrin–treated patients with IBD and specifically aimed to validate our previous findings from cohort 1, namely that in silico prediction of metabolic and ecological interactions associated with clinical efficacy in anti-TNF–treated patients with IBD.

Indeed, in silico predictions on bacterial interactions suggested differences in the gastrointestinal microbial ecology depending on the patients' remission status in response to anti-TNF. Only patients who did not achieve clinical remission displayed significantly reduced antagonistic interactions and significantly increased resource competitive interactions, when compared with HCs. Both findings were in line with findings from cohort 1, indicating that nonremitting patients with IBD display a disrupted gut microbial ecosystem (Figure 5*A*). Moreover, the baseline total predicted metabolic interchange (ie, cross-feeding)

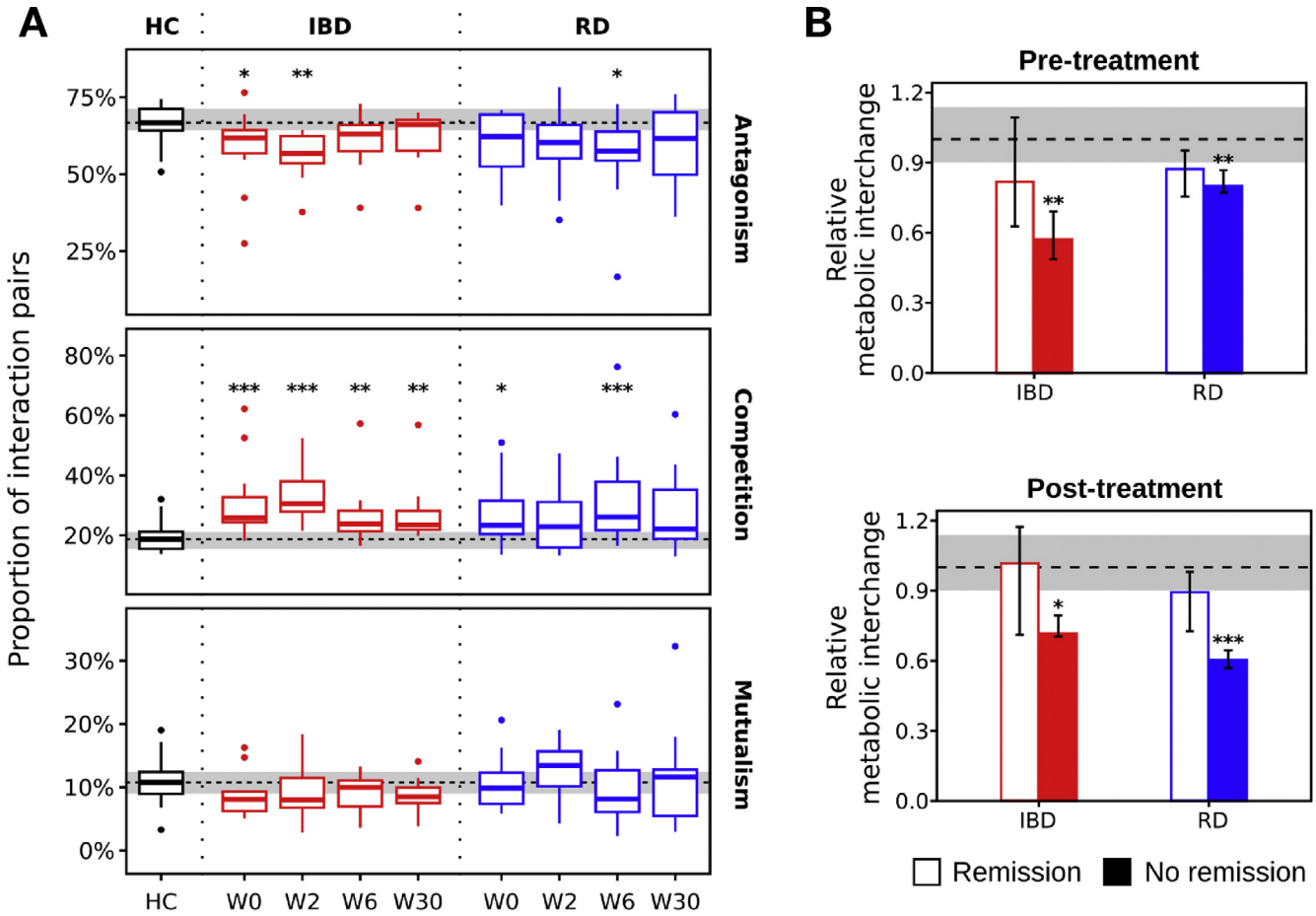

Figure 4. Bacterial metabolic interactions are disrupted in IBD and rheumatic diseases (RD), and metabolic interchange is especially reduced in patients not remitting in response to anti-TNF intervention. (*A*) Fraction of antagonistic (+/–), competitive (–/–), and mutualistic (+/+) interactions among bacterial community members for each disease group (IBD or RD) and therapy duration (week 0, 2, 6, or 30). Dashed lines indicate the median value for samples from healthy subjects and the gray area the interquartile range (IQR). (*B*) Predicted total intercellular metabolite fluxes (ie, interchange/cross-feeding) of all metabolites relative to HCs. The dashed line (= 1) indicates the median value and the gray area the IQR for samples from healthy subjects. Bar heights denote the median interchange estimates for the respective disease group (pretreatment vs posttreatment), depending on the patients' therapy response status (Remission vs No Remission). Error bars span the IQR. Asterisks indicate significantly different levels for the respective disease group and time compared with HCs (2-sided Mann-Whitney *U* test, $P < .05$).

was already reduced by 25% ± 5% (median ± SE) only in nonremitter IBD patients compared with HCs (Figure 5*B*, top; Mann-Whitney *U* test, $P = .02$), whereas the predicted metabolic interchange of remitter patients with IBD were similar to levels observed for controls (Figure 5*B*, bottom; Mann-Whitney *U* test, $P = 0.48$). To exclude any a priori confounding factors that might affect the predicted metabolic interchange, we performed linear regression of gut metabolic interchange with clinical, laboratory, and histology-based disease markers at baseline. We were not able to observe significant differences in disease activity parameters (HBI/Mayo at baseline, leukocytes, C-reactive protein, pathology index) that might explain different baseline metabolic interchange between remitting and nonremitting patients (Supplementary Figure 5). To assess whether disruption of metabolic interchange was specifically attributed to anti-TNF therapy or displayed a unifying phenomenon of clinical disease state, we investigated the proportion of metabolic interaction pairs between remitters and nonremitters in response to therapy induction with an anti $\alpha 4\beta 7$-integrin antibody (vedolizumab). Although the sample number of remitters (n = 11) and nonremitters (n = 2) was too small to substantiate our findings using a statistically valid method, our observation indicates that disrupted microbial metabolic interchange may also be more pronounced in nonremitters to vedolizumab (Supplementary Figure 6).

In Silico Meta-analysis of Microbial Metabolite Cross-Feeding Interactions Predicts Specific Metabolic Pathways Associated With Anti-TNF Therapy in IBD

To identify exact metabolite cross-feeding interactions that are disrupted during IBD, we combined the 16S rRNA data from all patients undergoing anti-TNF therapy in

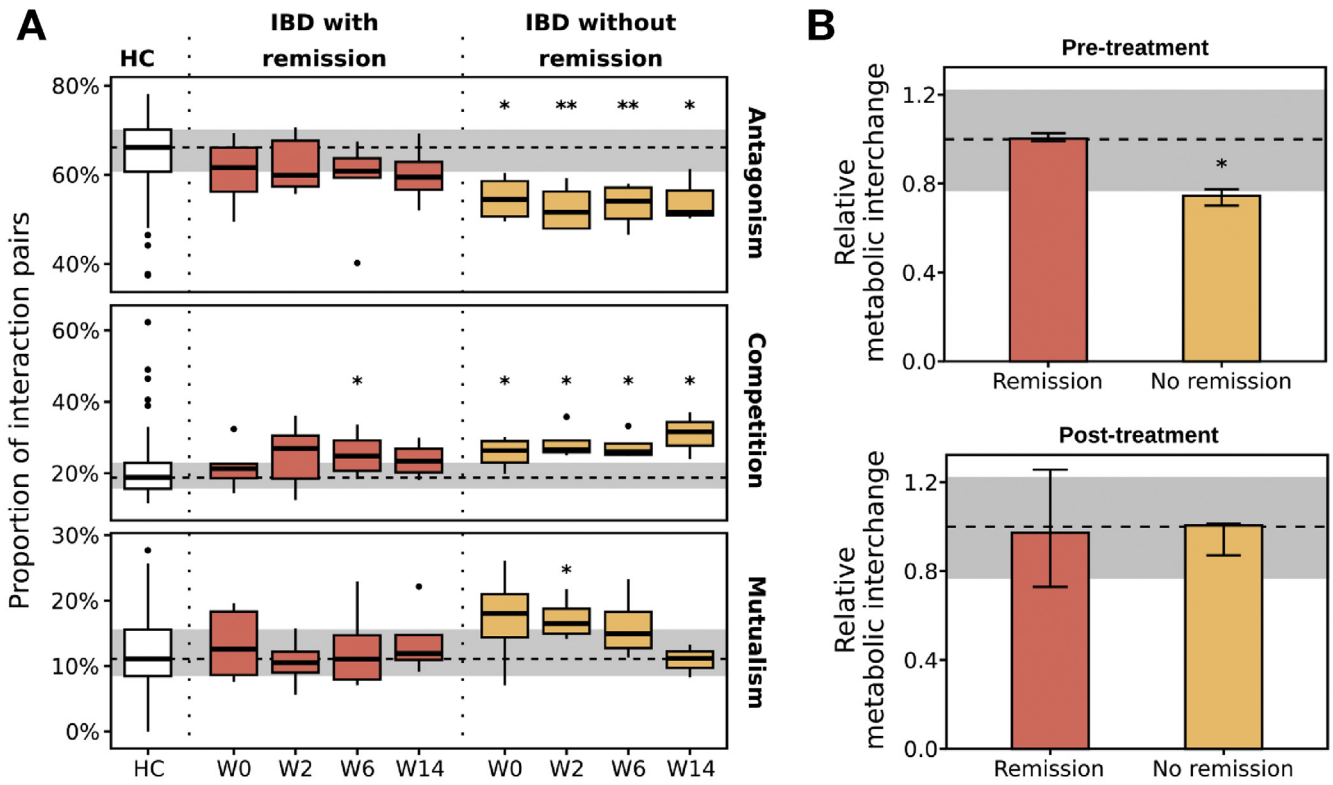

Figure 5. In silico–predicted ecological interaction types and total metabolite interchange levels in patients with IBD before and during anti-TNF intervention. (*A*) Fraction of antagonistic (+/–), competitive (–/–), and mutualistic (+/+) interactions among bacterial community members. Dashed lines indicate the median value for samples from healthy subjects and the gray area the interquartile range (IQR). (*B*) Predicted total intercellular metabolite fluxes (ie, interchange/cross-feeding) of all metabolites relative to the interchange levels in HCs. The dashed line (= 1) indicates the median value and the gray area the IQR for samples from healthy subjects. Bar heights denote the median of predicted interchange estimates for the respective disease group and the patients' remission status. Error bars span the IQR. Asterisks indicate significantly different levels for the respective disease group and time compared with HCs (2-sided Mann-Whitney *U* test, $P < .05$).

cohorts 1 and 2 for an in silico meta-analysis. Principal component analysis on the predicted cross-feeding rates of 374 metabolites revealed neither cohort-derived batch effects nor gender disparities (Supplementary Figure 7). From these cross-feeding interactions, we inferred 10 metabolites in nonremitter patients that were less frequently exchanged already at baseline compared with HCs. Only 3 (ethanol, glutamate, glycine) of them were also observable in patients who achieved clinical remission (Figure 6, left Venn diagram), suggesting a stronger disruption of the metabolic interaction network in nonremitter patients with IBD. Interestingly, in silico analysis predicted a restoration of some affected metabolites (eg, butyrate) after anti-TNF therapy (Figure 6, right Venn diagram). Overall, nonremitting patients with IBD display a stronger disruption of metabolic interactions (7 metabolites) in response to anti-TNF therapy compared with patients achieving clinical remission (4 metabolites, Figure 6). A direct comparison of baseline samples from remitting and nonremitting patients inferred that especially the intercellular exchange of butyrate is significantly reduced by 81% (median) in nonremitter patients compared with patients with IBD who achieved clinical remission (false discovery rate–corrected Mann-Whitney *U* test, $P = .02$). Overall, these results support the hypothesis that the response to therapy itself is strongly associated with the prevalence of metabolic exchanges in treatment-naïve patients.

Clinical Remission in Anti-TNF Therapy Is Associated With Changes in the Stool Metabolome

Based on the in silico prediction of gut microbial metabolic cross-feeding interactions, we postulated that anti-TNF therapy might also be associated with changes in fecal metabolites. To test this hypothesis, we investigated the stool metabolome from 9 patients with IBD (CD = 3, UC = 6, remitting = 5, nonremitting = 4) at baseline and after 14 weeks of anti-TNF treatment. To define which metabolites were characteristic in baseline, nonremission, and remission groups, we built an orthogonal partial least squares discriminant analysis model (Figure 7*A*). The classification models were highly significant for both datasets. Overall, we observed time-dependent differences between baseline and week 14 and fewer differences due to remission state (Figure 7*A* and *B*). Despite small effects of the treatment, we could find particular metabolites increased at baseline, in remission or in nonremission state (Figure 7*C*). Within the screening set of 50 metabolites (authentic chemical

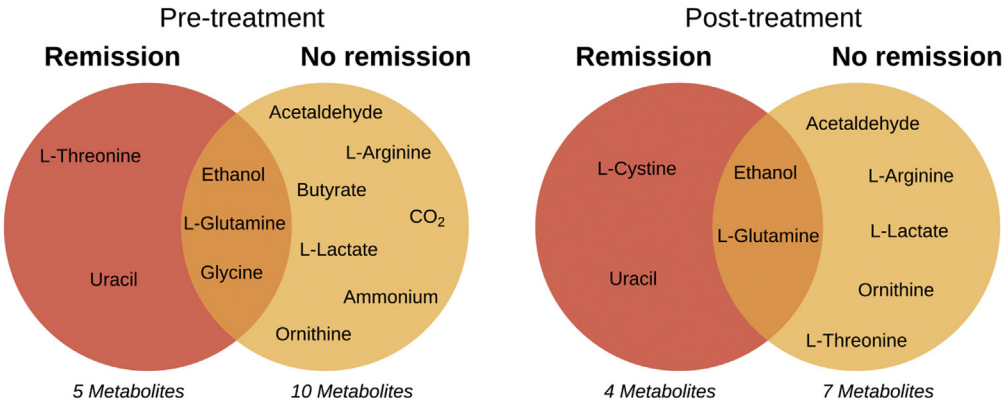

Figure 6. Disruption of specific metabolite exchange interactions between bacteria is more pronounced in nonremitter patients with IBD than in remitter patients already before anti-TNF therapy. The Venn diagrams show metabolites whose exchanges between bacterial community members are, compared with HCs, significantly reduced in patients with IBD who go into remission and/or do not achieve remission in the course of the treatment (left: before treatment; right: after treatment; false discovery rate–corrected 2-sided Mann-Whitney *U* test, $P < .05$). All anti-TNF–treated patients with IBD from cohorts 1 and 2 were combined for this analysis to improve statistical power.

standards), 21 were found in fecal samples and of those, 4 metabolites were responsible for the discrimination of the 3 groups (Figure 7*C*). Whereas the baseline group was discriminated by elevated levels of 3-indolepropionic acid and L-tyrosine, 3-hydroxyphenylacetic acid was increased in the remission group and pyruvic acid in the nonremission group (Figure 7*C*). All other clusters were not identified by an authentic chemical standard and are only putatively annotated on MS1 or MS2 level (summarized in Supplementary Table 8). We next investigated whether specific stool metabolites were applicable to delineate clinical remission in anti-TNF–treated patients with IBD. Overall, creatinine distinguished untreated (week 0) from anti-TNF–treated (week 14) patients, irrespective of remission status. Interestingly and in line with our in silico prediction, we found that butyric acid was significantly increased uniquely in the stool metabolome of anti-TNF remission patients. In contrast we found that the metabolite Cluster_1061 annotated as "3-methyl-thiopropionic acid, methyl 2-(methylthio)acetate" (Figure 7*F*) was found to be specifically increased in patients with IBD not achieving remission at week 14.

Discussion

Dysbiosis is defined by altered diversity, composition, and structure of the intestinal microbiota, but the underlying metabolic principles contributing to dysbiosis remain poorly understood. Most importantly, it is unknown whether anti-TNF therapy may affect gut microbial composition or function and could thereby contribute to disease control in IBD. In this study, we investigated the interplay of therapeutic anti-TNF inhibition and gut microbiota function in IBD and delineated the effects of organ-specific inflammation (ie, intestinal vs nonintestinal) on host microbe interaction using patients with rheumatic disease as a nonintestinal inflammatory control cohort. We confirmed that IBD and rheumatic diseases display distinct features of altered microbial community structure and metabolic function in comparison with healthy individuals and thereby confirm previous findings from studies assessing fecal global microbial profiles (α- and β-diversity) in IBD and rheumatic diseases.[11,30,31] Although these previously published studies used different techniques and sampling conditions, we present a coherent dataset as a direct side-by-side comparison of rheumatic diseases and patients with IBD recruited from the same clinical setting. Furthermore, we applied a novel systems biology approach that, for the first time in the context of IBD, allowed us to assess functional consequences of the dysbiotic change in community structure on the level of metabolic interactions within microbial communities. We show that anti-TNF treatment induces restoration of intestinal microbial diversity in IBD, whereas in rheumatic diseases, anti-TNF–associated changes were less pronounced and only transient. We further analyzed anti-TNF–associated shifts of phylotype abundances in IBD and rheumatic diseases by indicator species analysis and identified disease-specific phylotypes that change their abundance over the time course of anti-TNF treatment in either IBD or rheumatic diseases. Notably, we neither identified indicator species that specifically attributed to clinical efficacy of anti-TNF treatment nor did we confirm previously reported associations of increased counts of *Faecalibacterium prausnitzii* at baseline with therapeutic efficacy,[32] which both might be attributed to small sample sizes in our study.

It is noteworthy that phylotypes whose abundance changed significantly in patients with IBD toward the direction of healthy subjects (eg, *Coprococcus* and *Roseburia inulinivorans*) are known SCFA producers.[33,34]

These findings prompted us to interrogate gut metabolic functions using an in silico, 16S rRNA gene sequencing-based metabolic cross-feeding analysis. This analysis was conducted to identify metabolic cross-feeding interactions that might contribute to increased butyrate production observed in the case of therapeutic efficacy (remission). Using 2 independent cohorts of anti-TNF therapy in IBD, we assessed potential

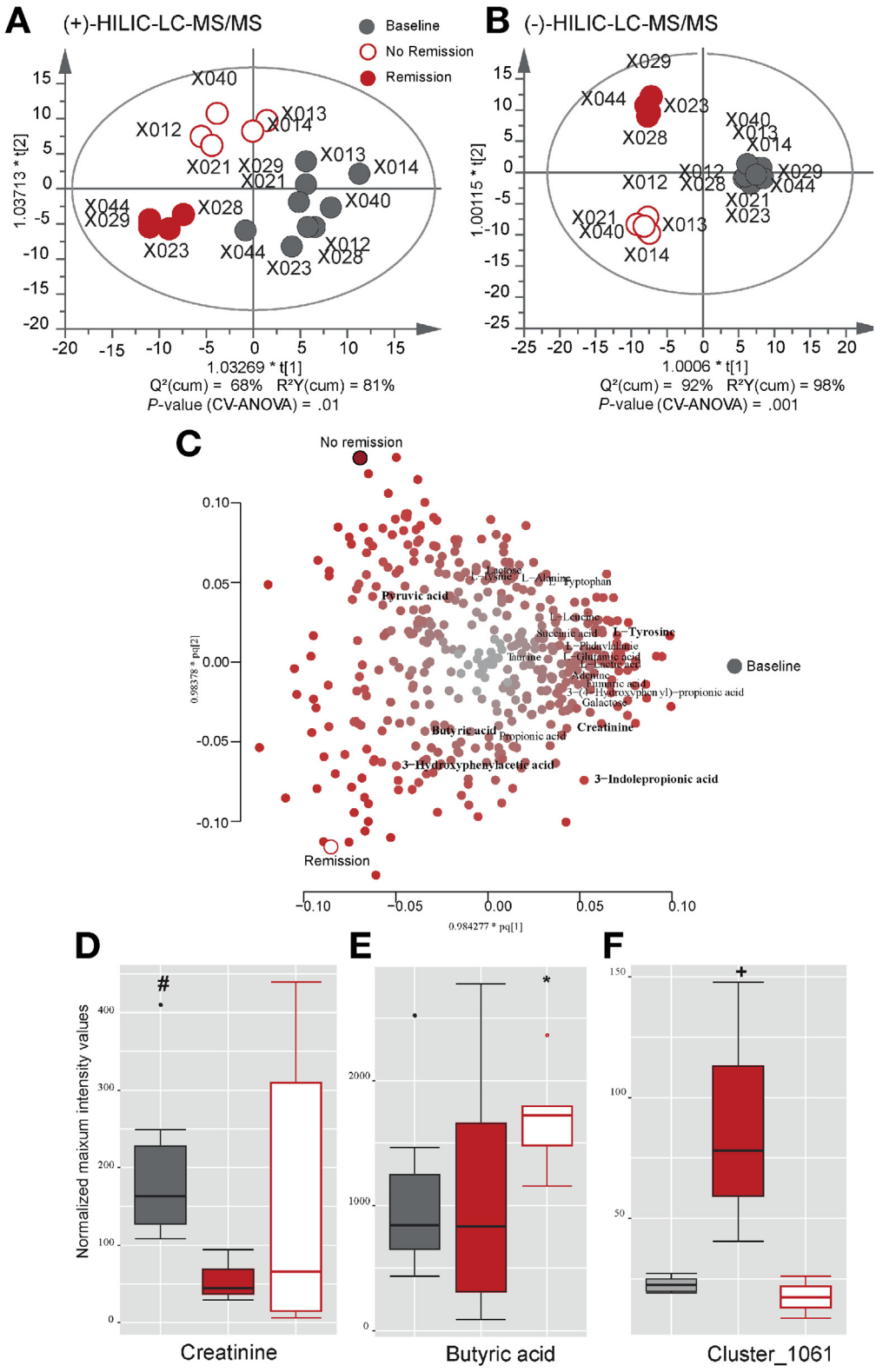

Figure 7. Stool metabolome analysis identifies indicator metabolites of therapy response in patients with IBD. Orthogonal partial least squares discriminant analysis (OPLS-DA) scores plot derived from (+)- (*A*) and (–)-hydrophilic interaction chromatography–liquid chromatography tandem mass spectrometry (HILIC-LC-MS/MS) (*B*) analysis of longitudinal stool samples of 9 patients with IBD, who underwent anti-TNF therapy. Samples were collected before therapy and at 14 weeks. Baseline, nonremission and remission samples are colored in gray and red, respectively. OPLS-loading plot illustrates clusters, which are responsible for the separation of the 3 groups. (*C*) Clusters are colored according to the importance for the 3 classes (red [high] to gray [low]). Metabolites identified by authentic chemical standards are labeled. (*D–F*) Creatinine, butyric acid, and the metabolite Cluster_1061 were found to be significantly altered between the groups. **#,** increased at baseline compared to the nonremission group; *****, increased in the remission group compared to baseline; **+**, increased in the nonremission group compared with remission group; significance was calculated with Mann-Whitney rank sum test ($P < .05$). CV-ANOVA, cross-validation analysis of variance.

metabolic interactions between bacteria within the community using constraint-based modeling. We show that reduction in metabolite cross-feeding interactions and increase of resource competition are present in IBD. Such metabolic interactions are widespread in human intestinal microbiota and are thought to be of high importance for community stability and robustness in a healthy state.[35] Although mutualistic and antagonistic interactions can stabilize community dynamics and thereby contribute to the maintenance of species diversity,[27,28] interspecific resource competition can reduce

community stability.[27] Moreover, it has been suggested that species co-occurrences in microbial communities are largely driven by metabolic exchanges between cells.[36] Indeed, we observed that metabolite exchange interactions could be restored by anti-TNF intervention in IBD. More importantly, we show that, already at baseline level, the total metabolite exchange across bacteria is significantly disrupted in patients with IBD not achieving clinical remission in response to anti-TNF therapy. Last, we found that butyrate and substrates involved in butyrate synthesis, such as ethanol or acetaldehyde, were less frequently exchanged among bacterial communities from patients who did not show therapeutic efficacy in response to anti-TNF therapy. Along this line, it has been shown by various studies that disturbances in the microbial networks containing taxa that typically produce SCFA characterize treatment failure to conventional and biologic therapy.[37,38] These findings do not only support the crucial role of SCFA in the disease control of patients with IBD but also underline the feasibility of using 16S in silico analysis to predict metabolic pathways that are disrupted in IBD and might affect therapeutic efficacy, which has also been suggested by others.[39,40] It is tempting to speculate on the mechanism of action by which biologic therapy is able to restore metabolite exchange interactions in IBD. A robust clinical response to biologic therapy leads to mucosal healing, inducing subsequent changes in host transcriptome architecture.[18] As impaired congruence between host transcriptome and gut microbiome has been described as a distinct feature of IBD,[41] we assume that reestablished congruence upon successful biologic therapy might also affect phylotype-phylotype interactions and metabolite crosstalk among bacteria. However, a further detailed molecular description of changes in the mucosa-associated microbiota and their interaction with host transcriptional changes in the context of anti-TNF treatment is needed to deepen our understanding of the host-microbial interaction and its effect on remission induction.

In summary, we demonstrate that the use of anti-TNF treatment leads to restoration of intestinal microbiome constitution and shifts of disease indicator taxa in human IBD, and we show that specific inferred metabolic interactions between luminal bacteria are associated with therapeutic outcome in IBD. Similar to studies on immune checkpoint inhibitors in cancer, our study clearly suggests functional links between the intestinal microbial ecosystem and therapeutic manipulation by TNF inhibition. Further studies are thus warranted to analyze the exact role of the microbial metabolic interaction network as a potential diagnostic marker or actionable entry point to actively improve therapy control in IBD.

Supplementary Material

Note: To access the supplementary material accompanying this article, visit the online version of *Gastroenterology* at www.gastrojournal.org, and at https://doi.org/10.1053/j.gastro.2019.07.025.

References

1. Schreiber S, Rosenstiel P, Albrecht M, et al. Genetics of Crohn disease, an archetypal inflammatory barrier disease. Nat Rev Genet 2005;6:376–388.
2. McInnes IB, Schett G. Cytokines in the pathogenesis of rheumatoid arthritis. Nat Rev Immunol 2007;7:429–442.
3. de Lange KM, Moutsianas L, Lee JC, et al. Genome-wide association study implicates immune activation of multiple integrin genes in inflammatory bowel disease. Nat Genet 2017;49:256–261.
4. Franke A, McGovern DPB, Barrett JC, et al. Genome-wide meta-analysis increases to 71 the number of confirmed Crohn's disease susceptibility loci. Nat Genet 2010;42:1118–1125.
5. Anderson CA, Boucher G, Lees CW, et al. Meta-analysis identifies 29 additional ulcerative colitis risk loci, increasing the number of confirmed associations to 47. Nat Genet 2011;43:246–252.
6. Salmond RJ, Brownlie RJ, Morrison VL, et al. The tyrosine phosphatase PTPN22 discriminates weak self peptides from strong agonist TCR signals. Nat Immunol 2014;15:875–883.
7. Spalinger MR, Lang S, Vavricka SR, et al. Protein tyrosine phosphatase non-receptor type 22 modulates NOD2-induced cytokine release and autophagy. PLoS One 2013;8:e72384.
8. Hevia A, Milani C, López P, et al. Intestinal dysbiosis associated with systemic lupus erythematosus. MBio 2014;5:e01548-14.
9. Costello M-E, Ciccia F, Willner D, et al. Brief report: intestinal dysbiosis in ankylosing spondylitis. Arthritis Rheumatol 2015;67:686–691.
10. Rehman A, Rausch P, Wang J, et al. Geographical patterns of the standing and active human gut microbiome in health and IBD. Gut 2016;65:238–248.
11. Gevers D, Kugathasan S, Denson Lee A, et al. The treatment-naive microbiome in new-onset Crohn's disease. Cell Host Microbe 2014;15:382–392.
12. Imhann F, Vich Vila A, Bonder MJ, et al. Interplay of host genetics and gut microbiota underlying the onset and clinical presentation of inflammatory bowel disease. Gut 2018;67:108–119.
13. Ott SJ, Musfeldt M, Wenderoth DF, et al. Reduction in diversity of the colonic mucosa associated bacterial microflora in patients with active inflammatory bowel disease. Gut 2004;53:685–693.
14. Vaahtuovuo J, Munukka E, Korkeamäki M, et al. Fecal microbiota in early rheumatoid arthritis. J Rheumatol 2008;35:1500–1505.
15. Chen J, Wright K, Davis JM, et al. An expansion of rare lineage intestinal microbes characterizes rheumatoid arthritis. Genome Med 2016;8:43.
16. Kalliolias GD, Ivashkiv LB. TNF biology, pathogenic mechanisms and emerging therapeutic strategies. Nat Rev Rheumatol 2016;12:49–62.
17. Ben-Horin S, Chowers Y. Tailoring anti-TNF therapy in IBD: drug levels and disease activity. Nat Rev Gastroenterol Hepatol 2014;11:243–255.

18. Zeissig S, Rosati E, Dowds CM, et al. Vedolizumab is associated with changes in innate rather than adaptive immunity in patients with inflammatory bowel disease. Gut 2019;68:25–39.
19. Vétizou M, Pitt JM, Daillère R, et al. Anticancer immunotherapy by CTLA-4 blockade relies on the gut microbiota. Science 2015;350:1079–1084.
20. Daillère R, Vétizou M, Waldschmitt N, et al. *Enterococcus hirae* and *Barnesiella intestinihominis* facilitate cyclophosphamide-induced therapeutic immunomodulatory effects. Immunity 2016;45:931–943.
21. Walmsley RS, Ayres RCS, Pounder RE, et al. A simple clinical colitis activity index. Gut 1998;43:29–32.
22. Yue JC, Clayton MK. A similarity measure based on species proportions. Commun Stat Theory Methods 2005;34:2123–2131.
23. Schloss PD, Westcott SL, Ryabin T, et al. Introducing mothur: open-source, platform-independent, community-supported software for describing and comparing microbial communities. Appl Environ Microbiol 2009; 75:7537–7541.
24. Dufrene M, Legendre P. Species assemblages and indicators species: the need for a flexible assymetrical approach. Ecol Monogr 1997;67:345–366.
25. Magnusdottir S, Heinken A, Kutt L, et al. Generation of genome-scale metabolic reconstructions for 773 members of the human gut microbiota. Nat Biotech 2017;35:81–89.
26. Turnbaugh PJ, Hamady M, Yatsunenko T, et al. A core gut microbiome in obese and lean twins. Nature 2008; 457:480.
27. Rohr RP, Saavedra S, Bascompte J. On the structural stability of mutualistic systems. Science 2014;345:416.
28. Mougi A, Kondoh M. Diversity of interaction types and ecological community stability. Science 2012;337:349–351.
29. Brandstetter BR, Korfmann A, Kroke A, et al. Dietary habits in the German EPIC cohorts: food group intake estimated with the food frequency questionnaire. Ann Nutr Metab 1999;43:246–257.
30. Vaahtovuo J, Munukka E, Korkeamäki M, et al. Fecal microbiota in early rheumatoid arthritis. J Rheumatol 2008;35:1500.
31. Zhang X, Zhang D, Jia H, et al. The oral and gut microbiomes are perturbed in rheumatoid arthritis and partly normalized after treatment. Nat Med 2015;21:895–905.
32. Magnusson MK, Strid H, Sapnara M, et al. Anti-TNF therapy response in patients with ulcerative colitis is associated with colonic antimicrobial peptide expression and microbiota composition. J Crohns Colitis 2016; 10:943–952.
33. Flint HJ, Duncan SH, Scott KP, et al. Links between diet, gut microbiota composition and gut metabolism. Proc Nutr Soc 2015;74:13–22.
34. Louis P, Hold GL, Flint HJ. The gut microbiota, bacterial metabolites and colorectal cancer. Nat Rev Micro 2014; 12:661–672.
35. Flint HJ, Duncan SH, Scott KP, et al. Interactions and competition within the microbial community of the human colon: links between diet and health. Environ Microbiol 2007;9:1101–1111.
36. Zelezniak A, Andrejev S, Ponomarova O, et al. Metabolic dependencies drive species co-occurrence in diverse microbial communities. Proc Natl Acad Sci U S A 2015; 112:6449–6454.
37. Yilmaz B, Juillerat P, Øyås O, et al. Microbial network disturbances in relapsing refractory Crohn's disease. Nat Med 2019;25:323–336.
38. Hyams JS, Davis Thomas S, Gotman N, et al. Clinical and biological predictors of response to standardised paediatric colitis therapy (PROTECT): a multicentre inception cohort study. Lancet 2019;393:1708–1720.
39. Bauer E, Thiele I. From metagenomic data to personalized in silico microbiotas: predicting dietary supplements for Crohn's disease. NPJ Syst Biol Appl 2018;4:27.
40. Graspeuntner S, Waschina S, Künzel S, et al. Gut dysbiosis with bacilli dominance and accumulation of fermentation products precedes late-onset sepsis in preterm infants. Clin Infect Dis 2019;69:268–277.
41. Häsler R, Sheibani-Tezerji R, Sinha A, et al. Uncoupling of mucosal gene regulation, mRNA splicing and adherent microbiota signatures in inflammatory bowel disease. Gut 2017;66:2087–2097.

Received February 28, 2019. Accepted July 4, 2019.

Reprint requests
Address requests for reprints to: Philip Rosenstiel, MD, Institute of Clinical Molecular Biology, University Hospital Schleswig-Holstein, Campus Kiel, Rosalind-Franklin-Straße 12, D-24105 Kiel, Germany, e-mail: p.rosenstiel@mucosa.de; fax: +49 (431) 500–12070; or Stefan Schreiber, MD, Department of Internal Medicine I., University Hospital Schleswig-Holstein, Campus Kiel, Rosalind-Franklin-Straße 12, D-24105 Kiel, Germany, e-mail: s.schreiber@mucosa.de; fax: +49 (431) 500-15104.

Acknowledgments
The authors thank all the participating patients for supporting this study by donating biomaterial. The expert technical assistance by Karina Greve and Dorina Oelsner, as well as the scientific support by Markus Schilhabel and Sören Franzenburg, are gratefully acknowledged. We thank Ines Thiele, Eugen Bauer, and Almut Heinken for valuable discussions concerning constraint-based modeling of microbial communities.

Author contributions: KA and PR designed the study; KA, SN, JOS, RZ, and JB collected biosamples and performed clinical scoring; AR, WHP, RB, SW, and JZ performed sequencing and analysis; SW, JZ, CK, DV, and JR performed in silico analysis of bacterial community assembly and metabolism; AW and PSK performed metabolomics; CK, JR, SSz, GHW, and AF performed critical revision of the manuscript for important intellectual content; KA, AR, SW, JZ, CK, SS, and PR wrote the manuscript.

Conflicts of interest
Konrad Aden has received funding from Pfizer (Germany) to execute parts of this study. The grant did not affect study design at any time point. GHW is an employee of the Conaris Research Institute AG, the employment did not affect his contribution to this study. The remaining authors disclose no conflicts.

Funding
This work was funded by the BMBF-initiative E:med sysINFLAME, the Clusters of Excellence Inflammation at Interfaces and Precision Medicine in Chronic Inflammation (ExC 306 and 2167), the EU H2020 SYSCID program under the grant agreement No 733100, and the DFG (SCHR 512/14–1).

Supplementary Materials and Methods

16S rRNA Gene Sequencing

Aliquot of extracted DNA was used to amplify V4 variable region of 16S rRNA gene. Forward primer (515F) consists of 5′ Illumina (San Diego, CA) adaptor (AATGATACGGCGACCACCGAGATCTACAC), a primer pad (TATGGTAATT), linker (GT), and 16S rRNA gene-specific forward primer (GTGCCAGCMGCCGCGGTAA) and reverse primer (806R) includes reverse complement of 3′ Illumina adapter (CAAGCAGAAGACGGCATACGAGAT) a 12-nucleotide barcode (xxxxxxxxxxxx) reverse primer pad (AGTCAGTCAG), reverse primer linker (CC) and reverse primer (GGACTACHVGGGTWTCTAAT). 16S rRNA gene variable region V3 and V4 will be amplified using dual-indexed fusion primers.[1] In brief, primers consist of illumina linker sequence, 12 base barcode sequence, and heterogeneity spacer followed by either 16S rRNA gene-specific forward (319F: ACTCCTACGGGAGGCAGCAG) or reverse (806R: GGACTACHVGGGTWTCTAAT) primer sequences. Amplification was performed by Phusion Hot start Flex 2X master Mix (New England Biolab, Frankfurt am Main, Germany) in GeneAmp Polymerase Chain Reaction (PCR) system 9700 (Applied Biosystems, Foster City, CA) using the following cycling conditions: an initial denaturation of 3 minutes at 98°C followed by 30 cycles, denaturation at 98°C for 10 seconds, annealing at 55°C for 30 seconds, elongation at 72°C for 30 seconds, and a final extension at 72°C for 10 minutes. PCR performance for quality (expected amplicon size) and quantity (band intensity) was assessed by running aliquot of amplified products on agarose gel. Quantitative normalization was performed using SequalPrep kit (Invitrogen, Carlsbad, CA) to pool equal amount of amplicons per sample. Sequencing was performed using the Illumina MiSeq platform employing a paired end approach with 2 times 250 bases, aiming at a 250 base target region. Consequently, this approach ensures the highest contig quality possible.

DNA Extraction and 16S rRNA Gene Sequencing

16S rRNA gene variable region V4 19 (cohort 1) and V3-V420 (cohort 2) –based bacterial profiles were generated from patients with IBD and patients with rheumatic diseases (RD) and HC feces. Total genomic DNA was extracted from feces using MoBio Powersoil DNA Isolation kit (Dianova GmbH, Hamburg, Germany) as per the manufacturer instructions. 16S rRNA gene amplicon libraries were prepared and sequenced as published earlier.

16S rRNA Gene Sequence Analysis

Sequencing reads were primarily processed for quality control using the software mothur package 21. For cohort 1, more than 2.2 million high-quality reads varying from 6366 to 67699 reads per samples. These sequences were binned into 453 taxonomical phylotypes. For subsequent analysis, sequences per sample were rarefied to 6366 to have comparable sequencing depth. This resulted in the rarefication of 388 phylotypes. For cohort 2, more than 2.7 million high-quality ready varying from 4036 to 43033 reads per samples. These sampels were binned into 441 taxonomical phylotypes.

Forward and reverse reads (fastq) were merged to form contigs, and discarded if they were more than 275 bases in length, having any ambiguous base, or more than 8 homopolymers. Sequences were aligned against mothur curated silva alignment database and screened to have alignment in amplified specified (V4, V3-V4) regions only. Chimeric sequences were detected by the Uchime 22 algorithm and were also removed. In the first step, sequences were classified (threshold 80%) phylogenetically using mothur formatted greengenes (gg_13_8_99) training sets and eliminated if classified as unknown, archaea, eukaryotes, chloroplast, or mitochondria. Subsequently, reference-based (green genes) operational taxonomical units (OTUs or phylotypes) picking approach was implemented to cluster sequences with same phylogenetic affiliations into a phylotype (label = 1).[2–5] Alpha diversity indices including observed and estimated number of phylotypes and nonparametric Shannon index were calculated using mothur. For phylogenetic diversity estimation, neighbor joining phylogenetic tree was generated by Clearcut command as implemented in mothur. Significance of differences in diversities among healthy, IBD, and RD subjects were assessed by Whitney *U* test, otherwise significance of differences in diversities before and after therapies were assessed by Wilcoxon matched-pairs signed-rank test. Both tests were performed in GraphPad prism 5.0 (GraphPad, La Jolla, CA). To identify the specific phylotypes that alters after therapy initiations, we used indicator species analysis24 using 1000 iteration using mothur.

Microbial Community Modeling

We used a flux balance analysis-based community modeling approach[6] to assess the functional consequences of shifts in microbial community structure in inflammatory diseases. Flux balance analysis is a methodological framework that tries to infer fluxes within metabolic networks through the utilization of comprehensive reconstructions of an organism's metabolic network and the assumption of evolutionary objectives for inferring fluxes within this network. The underlying metabolic networks used are typically built from the annotated genome of an organism with a downstream manual curation procedure that corrects errors in the model (eg, based on literature data), removes gaps in metabolic pathways, and performs distinct validation steps depending on the amount of experimental data available for a specific organism.[7] In addition, these networks contain information about the reversibility of the present reactions and information about the specific nutritional environment of an organism that is implemented through constraints on specific metabolite uptake and secretion reactions. Using such networks, flux balance analysis assumes that all (internal) metabolites within a metabolic network are balanced in their production/consumption and that irreversible reactions are used only in

the thermodynamically feasible direction. Using this assumption, flux balance analysis determines a flux that maximizes the production of all biomass components from the constrained nutrient supply, which should reflect the evolutionary objective of maximizing growth rate. In the context of microbial community modeling, the metabolic networks of distinct bacterial species are connected to each other through a common compartment that allows for the exchange of metabolites and contains an inflow of metabolites representing the respective growth environment considered (eg, a specific diet). We here assume that within a community, the objective of optimization is community growth, that is, the maximization of the total amount of bacterial biomass that is being produced.[8]

We used the AGORA (Assembly of Gut Organisms through Reconstruction and Analysis) resource containing genome-scale metabolic models of 773 constituent bacterial species of the human gut microbiota[8] to predict the ecological relationships between the species that are present in the analyzed microbial communities. These models were built in a semi-automated fashion from the annotated genomes of the corresponding species.[8] Furthermore, the models were used to assess the metabolic activity of communities in the individual samples under defined dietary conditions and oxygen regimes.[8] To simulate the nutritional environment in the human gut, the inflow of metabolites into the models were constrained by assuming a western diet and anaerobic conditions.[8]

Please note that in this study, the bacterial genome-scale metabolic models were used to predict metabolic phenotypes of bacterial populations within the sampled microbiomes. Therefore, predictions should be considered as novel hypothesis on the biochemical physiology of dysbiosis and need to be experimentally scrutinized in future studies.

Prediction of Bacterial Growth and Ecological Relationships

To determine whether pairs of coexisting species affect each other's metabolism and growth, we used Flux Balance Analysis[9] to predict the organisms' growth rates in isolation (single growth μ_{sg}) and their growth rates in pairs of different species (co-growth μ_{cg}). The underlying rationale is that the growth rate of an organism can be altered through metabolic interactions with neighboring cells. For co-growth simulations, the models were merged in a pairwise manner as previously described.[8,10] The predicted single growth and co-growth rates were compared to infer the theoretical ecological relationship of each pair of species: The relationship of 2 bacterial organisms was considered (1) *mutualistic* if each organism could grow faster in co-growth compared with single growth ($\mu_{cg} > \mu_{sg} + \varepsilon$), (2) *competitive* if both organisms grew slower compared with their respective single growth rate ($\mu_{cg} < \mu_{sg} - \varepsilon$), (3) *antagonistic* if one organism could grow faster while the other organism had a reduced growth rate, (4) *commensal* if one species could grow faster in a pair and one did not show an altered growth rate ($\mu_{sg} + \varepsilon > \mu_{cg} > \mu_{sg} - \varepsilon$) , (5) *amensal* if one organism had a reduced growth rate and the other organism's growth remained unchanged, and (6) *neutral* if both species showed no difference between single- and co-growth rate. An ε of 10^{-6} was used to account for minor differences between predicted single- and co-growth rates that might occur due to unstable floating-point computations during linear optimization. In this study, we focused on mutualistic, competitive, and antagonistic interactions because only less than 1% (median) of the species pairs per sample were predicted to be commensal, amensal, or neutral. All scripts for single- and co-growth simulations were implemented in R and are available at https://github.com/jotech/agora_interactions.

To map 16S sequencing reads from each sample to the corresponding bacterial models from the AGORA resource and their predicted interactions, sequence reads were aligned against the 16S ribosomal rRNA gene sequences of the corresponding bacteria using USEARCH.[11] Each sequence was mapped to the AGORA organism with the highest V4 16S sequence identity and sequence reads with less than 97% sequence identity were considered as bacteria that are not included in the AGORA collection. Next, we mapped for each sample the relative phylotype frequencies to every pair of AGORA organisms to calculate the relative pair abundancy $c_{i,i} = c_i^2$ and $c_{i,j} = 2 * c_i \cdot c_j$, for $i \neq j$, where c_i and c_j are the relative abundancies of the individual phylotypes i and j, respectively.

Prediction of Metabolic Interchange Within Bacterial Communities

To assess metabolic activity of the microbial communities for each sample, the metabolic models of bacteria mentioned previously were joined into a community simulation as described previously.[8,10] Only bacterial species that were detected with a relative abundance above 0.1% were included in the community model. To account for individual abundances, a "community biomass reaction" was introduced that incorporated the biomass reactions of the individual bacteria in accordance with their relative abundances. Fluxes were determined using parsimonious flux balance analysis,[12] by maximizing the production of community biomass subject to the previously mentioned dietary constraints and concomitantly minimizing the total sum of fluxes (scaled with a factor of 10^{-5} in the objective function). For each case, optimality of the resulting objective function value was verified by maximizing biomass production without minimization of the total sum of fluxes. To accelerate computation, dietary constraints were scaled by a factor of 10. For individual bacteria, active reactions were determined based on a threshold flux of 10^{-6} mmol/gDW per hour. To predict the activity of specific reactions on the community level, all fluxes of the same biochemical reactions across all community members were summed and a threshold flux of 10^{-4} mmol/gDW per hour was used to decide which reactions are likely to be active and which are not, or only marginally used. For the 2 cohorts we tested for significantly different predicted reaction activities between male and female samples within the healthy or IBD cohorts (pretreatment) but did not observe significant differences.

Impact of Different Assumptions for Dietary Conditions

As mentioned previously, the flux balance simulations for bacterial community metabolism requires the definition of the nutritional environment. Chemical composition of the environment of gut-inhabiting bacteria is decisively determined by the dietary habits of the human host.[13] Thus, also the model prediction might be strongly influenced by the nutritional assumptions for in silico simulations. Because all patients and healthy persons who were part of this study were located in northern Germany, we assumed a standardized western diet as defined previously.[8] Nonetheless, for sake of completeness, we compared the model predictions on the frequency on antagonistic, mutualistic, and resource competitive interactions also to a fictive diet high in fibers, such as arabinogalactan and xylan.[8] For healthy controls, the models predict less antagonistic and competitive interactions compared with western diets (see Figure 3A). In contrast to western diets, levels of antagonistic interactions in IBD and RD did not significantly differ from HCs, but resource competitive interactions were still significantly more frequent in both disease entities if a high-fiber diet is used for model simulations. Thus, changing the dietary conditions had some impact on model predictions, but model simulations do not contradict the central observation of more abundant community-destabilizing competitive interactions during disease. Moreover, assuming a western diet is more accurate for the specific 2 cohorts used in this study.

Manual and Literature-based Corrections to AGORA Metabolic Models

While in silico simulating the metabolic processes within bacterial communities, we came across a number of inconsistencies in the original models (Version 1.01) that caused unrealistically high predicted flux rates for metabolic cross-feeding interactions (ie, > 500 mmol*h^{-1}*gDW^{-1}; in comparison, the maximum inflow flux of water is set to 10 mmol*h^{-1}*gDW^{-1}). These high fluxes were caused by futile cycles that involved the cyclic release and uptake of metabolites as depicted in the scheme shown in Supplementary Figure 7. The corrections listed in Supplementary Table 6 prevented such cycles and include amendments in reaction stoichiometry and reversibility.

Statistical Analysis of Metabolomic Data

Metabolites were analyzed from stool samples of 9 subjects with IBD, treated with anti-TNFα antibody, which resulted in 4 nonremission and 5 remission patients at week 14. An orthogonal partial least squares discriminant analysis (OPLS-DA) was applied to find variables responsible for the separation of remission and nonremission patients before and after the treatment.

The robustness of the build model was verified by calculation of *P* values with cross-validation analysis of variance (CV-ANOVA). The goodness of fit R^2Y(cum), the goodness of prediction Q^2(cum), and the *P* values were reported as indicators for the significance of the models. The coefficients of regression of the models were considered to detect which metabolites are highly correlated (positively or negatively) with the different classes. All the classification models were done in SIMCA 13.0.3.0 (Umetrics, Umeå, Sweden), the box plots in RStudio (Version 1.0.136; 2009–2016, RStudio, Inc.) and the Mann-Whitney Rank Sum Test in SigmaPlot 12.0 (Systat Software Inc., San Jose, CA).

Nontargeted Metabolomics Using Hydrophilic Interaction Chromatography–Liquid Chromatography Tandem Mass Spectrometry

Approximately 50 mg of fecal stool sample was weighed in sterile ceramic bead tubes (NucleoSpin Bead Tubes, Macherey-Nagel, Dueren, Germany). One milliliter of prechilled (-20°C) methanol (LiChrosolv, hypergrade for liquid chromatography–mass spectrometry [LC-MS]; Merck KGaA, Darmstadt, Germany) was added to the stool sample and homogenized with Precellys Evolution Homogenizer (Bertin Corp., Rockville, MD; 4500 rpm, 40 $\times$ 3 seconds, 2-second pause time). Samples were then centrifuged for 10 minutes at 21,000*g*, and cooled at 4°C. An aliquot of 100 μL was evaporated at 40°C (Savant, SPD121P, SpeedVac Concentrator; ThermoFisher Scientific, Waltham, MA) and reconstituted with 75% acetonitrile (LiChrosolv, hypergrade for LC-MS; Merck KGaA) to perform hydrophilic interaction LC (HILIC) coupled to MS analyses. The robustness of the build model was verified by calculation of *P* values through the analysis of variance of the cross-validated predictive residuals (CV-ANOVA). To exclude possible overfitting, the significance level of *P* value was set to .05.

Fecal samples and standard mixtures of 50 metabolites were analyzed on a time of flight mass spectrometer (maXis; Bruker Daltonics, Bremen, Germany), coupled to an UHPLC system (Acquity; Waters, Eschborn, Germany). A charge modulated hydroxyethyl Amide HILIC column (iHILIC-Fusion UHPLC Column, SS, 100 $\times$ 2.1 mm, 1.8 μm, 100Å; HILICON AB, Umeå, Sweden) was used to separate polar metabolites of stool samples. A stock solution of 0.5 molar ammonium acetate (Merck KGaA) was adjusted to pH 4.6 with glacial acetic acid (Biosolve, Valkenswaard, Netherlands). MilliQH_2O was derived from Milli-Q Integral Water Purification System (Billerica, MA). Mobile phase for HILIC separation consisted of 5 mM ammonium acetate in 95% acetonitrile, pH 4.6 (A) and 25 mM ammonium acetate in 30% acetonitrile, pH 4.6 (B). Elution of metabolites was performed with a flow rate of 0.5 mL/minutes, using a 0.1% to 99.9% phase B gradient over 7.5 minutes. At the start, 0.1% B was kept for 2 minutes with increasing step to 99.9% B within 7.5 minutes; 99.9% B was constant for 2.5 minutes with fast decrease to 0.1% B within 0.1 minutes and a pre-run time of 2.5 minutes at 0.1% B. The column oven temperature was set to 40°C and the injection volume at partial loop was 5 μL.

MS Conditions

Internal calibration of mass spectrometer was done by injecting ESI-L Low Concentration Tuning Mix (Agilent, Santa Clara, CA). External calibration of mass spectrometer was ensured by injecting ESI-L Low Concentration Tuning Mix (1:4 diluted in 75% acetonitrile) in the first 0.3 minutes of each LC-MS run, introduced by a switching valve.

Mass spectra were acquired in positive and negative ionization mode (+/− ESI). ESI parameters were as follows: nitrogen flow rate of 10 L/minute, dry heater of 200°C, nebulizer pressure of 2.0 bar, and capillary voltage of 4500V. Data were acquired in line and profile mode with acquisition rate of 5 Hz. Data-dependent MS/MS experiments were performed for each sample by fragmenting the 3 most intense ions within 1 scan (>2000 counts, active exclusion of 3 spectra, release after 0.1 minute and reconsider precursor if current intensity/previous intensity × 3). Collision energy was set to 10 eV and isolation width of 8 Dalton.

Data Processing

Raw LC-MS data were processed with Genedata Refiner MS software (Genedata GmbH, Munich, Germany), including chemical noise substraction, calibration, chromatographic peak picking, deisotoping and metabolite library search (HMDB for MS1 level [±0.005 Dalton])[14] and spectral libraries derived from MassBank of North America (http://mona.fiehnlab.ucdavis.edu), including MassBank,[15] GNPS,[16] HDMB, and LipidBlast[17] for MS2 level (0.1 Dalton). Final data matrix consisted of mass signals (m/z) and their respective retention time (RT) in minutes, called cluster with observed maximum intensity for each sample. Clusters with RT <1 minute were excluded from further analysis. Data were normalized to the wet sample weight and scaled (unit-variance) before statistical analysis.

Supplementary References

1. Caporaso JG, Lauber CL, Walters WA, et al. Ultra-high-throughput microbial community analysis on the Illumina HiSeq and MiSeq platforms. ISME J 2012;6:1621.
2. Sul WJ, Cole JR, Jesus Eda C, et al. Bacterial community comparisons by taxonomy-supervised analysis independent of sequence alignment and clustering. Proc Natl Acad Sci U S A 2011;108:14637–14642.
3. Guss AM, Roeserlers G, Newton IL, et al. Phylogenetic and metabolic diversity of bacteria associated with cystic fibrosis. ISME J 2010;5:20.
4. Bradley IM, Pinto AJ, Guest JS. Design and evaluation of Illumina MiSeq-Compatible, 18S rRNA gene-specific primers for improved characterization of mixed phototrophic communities. Appl Environ Microbiol 2016; 82:5878–5891.
5. Al-hebshi NN, Nasher AT, Maryoud MY, et al. Inflammatory bacteriome featuring Fusobacterium nucleatum and Pseudomonas aeruginosa identified in association with oral squamous cell carcinoma. Sci Rep 2017; 7:1834.
6. Orth JD, Thiele I, Palsson BØ. What is flux balance analysis? Nat Biotechnol 2010;28:245.
7. Gudmundsson S, Thiele I. Computationally efficient flux variability analysis. BMC Bioinformatics 2010;11:489.
8. Magnusdottir S, Heinken A, Kutt L, et al. Generation of genome-scale metabolic reconstructions for 773 members of the human gut microbiota. Nat Biotech 2017; 35:81–89.
9. Savinell J, Palsson B. Network analysis of intermediary metabolism using linear optimization. I. Development of mathematical formalism. J Theor Biol 1992;154:421–454.
10. Heinken A, Sahoo S, Fleming RMT, et al. Systems-level characterization of a host-microbe metabolic symbiosis in the mammalian gut. Gut Microbes 2013;4:28–40.
11. Edgar RC. Search and clustering orders of magnitude faster than BLAST. Bioinformatics 2010;26:2460–2461.
12. Lewis NE, Hixson KK, Conrad TM, et al. Omic data from evolved E. coli are consistent with computed optimal growth from genome-scale models. Mol Syst Biol 2010; 6:390.
13. Kau AL, Ahern PP, Griffin NW, et al. Human nutrition, the gut microbiome and the immune system. Nature 2011; 474:327.
14. Wishart DS, Feunang YD, Marcu A, et al. HMDB 4.0: the human metabolome database for 2018. Nucleic Acids Res 2018;46:D608–D617.
15. Horai H, Arita M, Kanaya S, et al. MassBank: a public repository for sharing mass spectral data for life sciences. J Mass Spectrom 2010;45:703–714.
16. Wang M, Carver JJ, Phelan VV, et al. Sharing and community curation of mass spectrometry data with Global Natural Products Social Molecular Networking. Nat Biotechnol 2016;34:828.
17. Kind T, Liu KH, Lee DY, et al. LipidBlast in silico tandem mass spectrometry database for lipid identification. Nat Methods 2013;10:755.

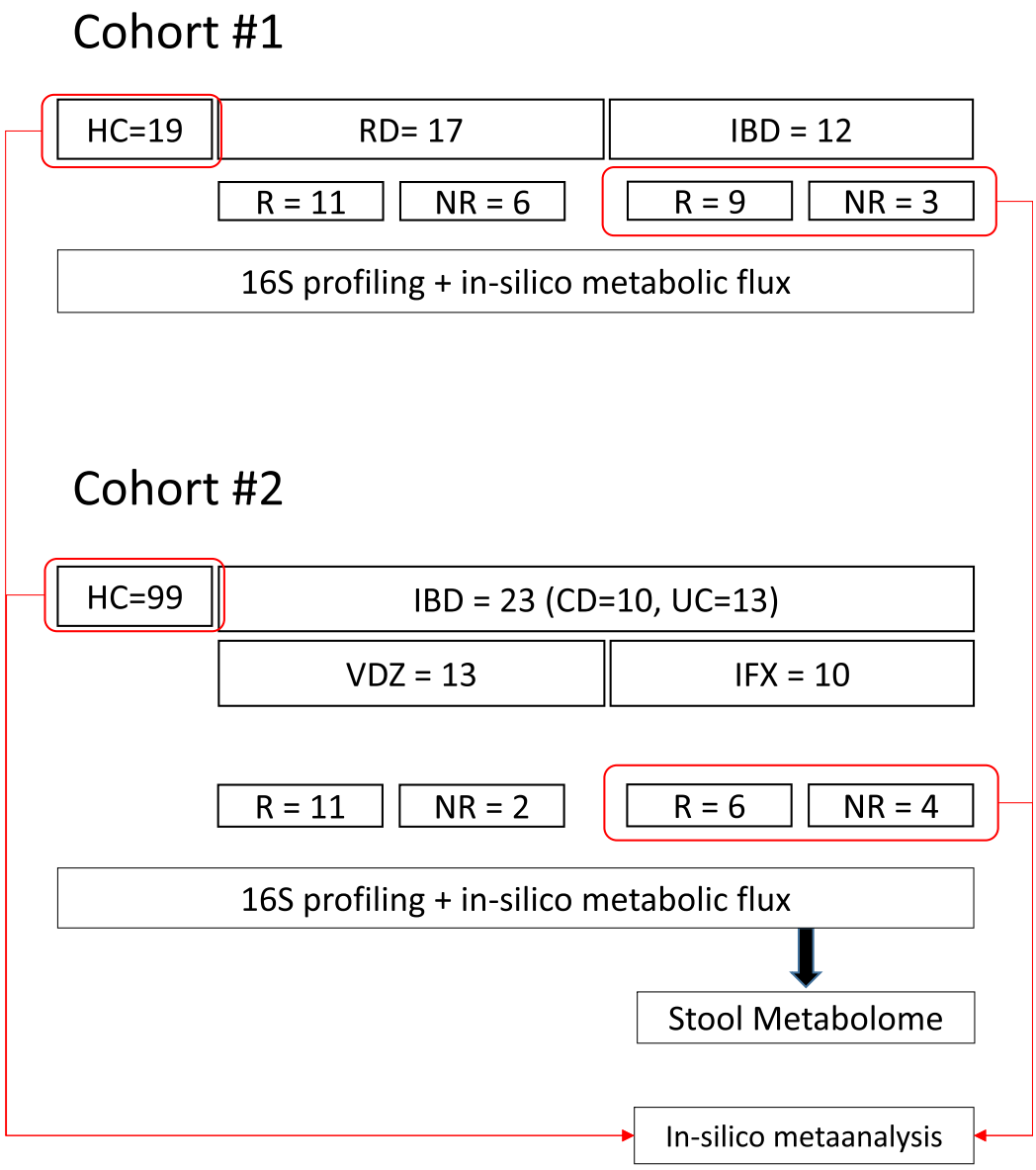

Supplementary Figure 1. Schematic overview of included cohort and analysis workflow. For hypothesis generation cohort 1 (MAUT) was included in 16S profiling + in silico metabolic flux analysis. Key findings were validated in cohort 2 (EMED). For in silico meta-analysis (Figure 6) HC (in total n = 118) and patients with IBD (in total n = 35) were pooled from cohorts 1 and 2.

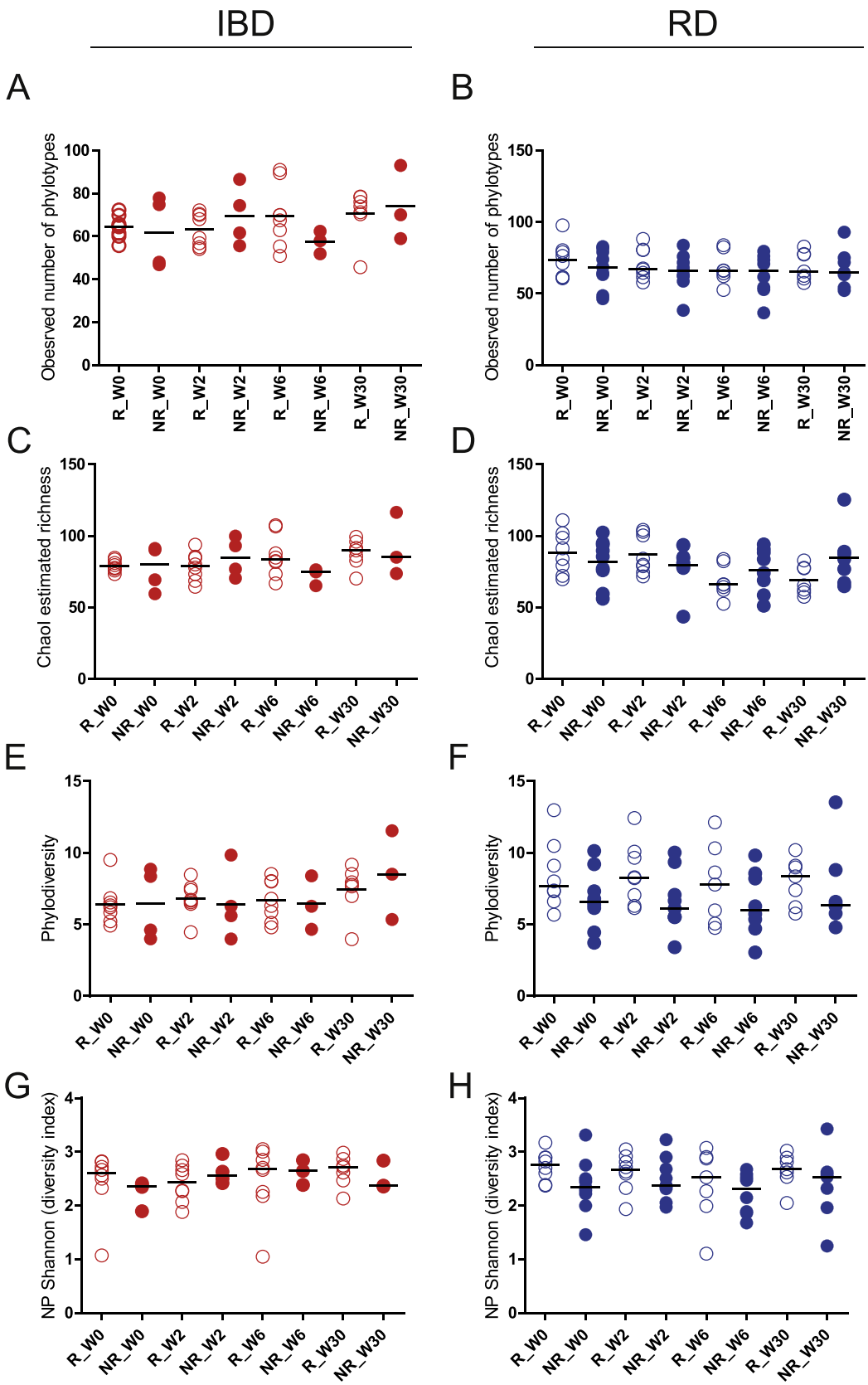

Supplementary Figure 2. Alpha diversity in patients with IBD and patients with rheumatic diseases (RD) according to responder status. As a measure of change in alpha diversity, observed number of phylotypes (*A* and *B*), estimated species richness (*C* and *D*), phylo-diversity (*E* and *F*), and NP Shannon diversity (*G* and *H*) were assessed in fecal samples collected from IBD and RD subjects at baseline and after initiation of anti-TNFα interventions. Responders are shown as open circles, whereas nonresponders are shown as filled circles.

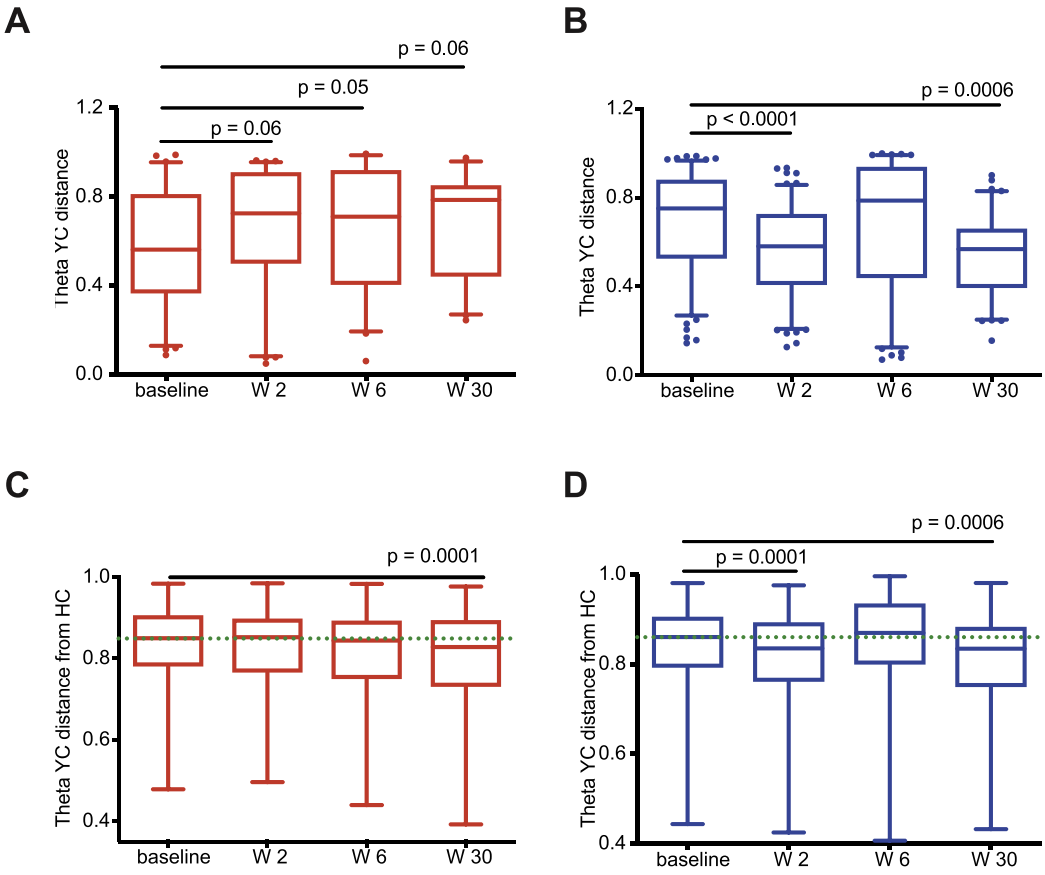

Supplementary Figure 3. Anti-TNFα therapeutic intervention induces expansion of beta diversity in IBD but not in RD. Yue and Clayton dissimilarity (beta diversity) within IBD (*A*) and RD (*B*) groups before and after anti-TNFα interventions. Interindividual distances before therapy initiation were used as baseline point to compare interindividual distances at week 2, week 6, and week 30 after anti-TNFα intervention. *P* values were determined by Wilcoxon matched-pairs signed-rank test and represent Yue and Clayton dissimilarity between HC and patients with IBD (*C*), HC and patients with RD (*D*). Interindividual distances were compared with HCs at baseline and after therapy initiation at week 2, week 6, and week 30. Significance of changes were ascertained by Mann-Whitney test.

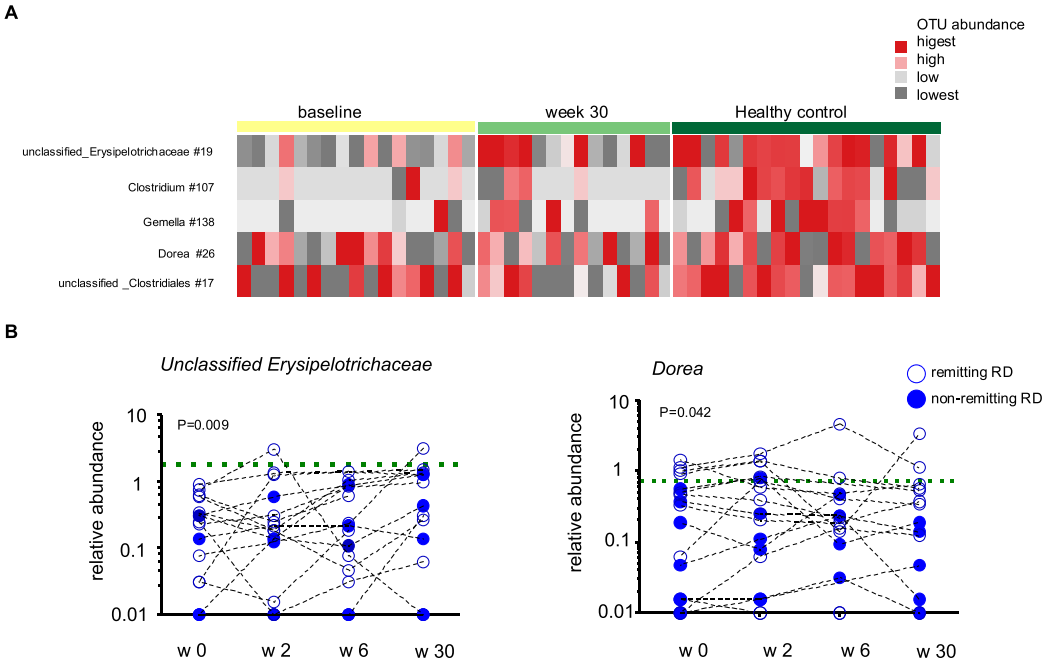

Supplementary Figure 4. Indicator phylotypes before and after anti-TNFα therapeutic intervention in patients with RD. (*A*) Loss (down) or gain (up) of indicator species status was determined in relation to healthy control group microbiota. Relative abundance signal values were transformed in to Z-score for visualization. Each column represents individual patients whereas each row represents the relative abundance of labeled indicator species. (*B*) Representative indicator phylotypes, that were significantly decreased at week 0 compared with HC and increased in abundance after anti-TNFα therapeutic intervention to become comparable to HC subject status at week 30. *P* values indicate the statistical significance at week 0 between patients with RD and HCs.

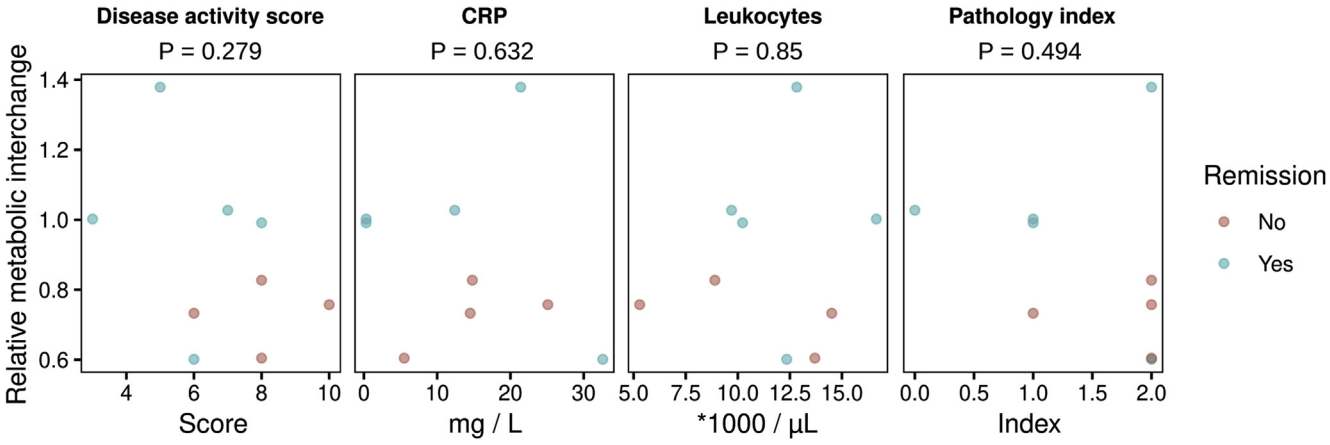

Supplementary Figure 5. Linear regression analysis of gut metabolic interchange with disease activity parameters at baseline. Linear regression of relative metabolic interchange with disease activity score (HBI/Mayo), leukocyte count, C-reactive protein, and pathology index. Note, that none of the listed parameters shows a significant relationship with the degree of relative metabolic interchange in baseline microbial samples.

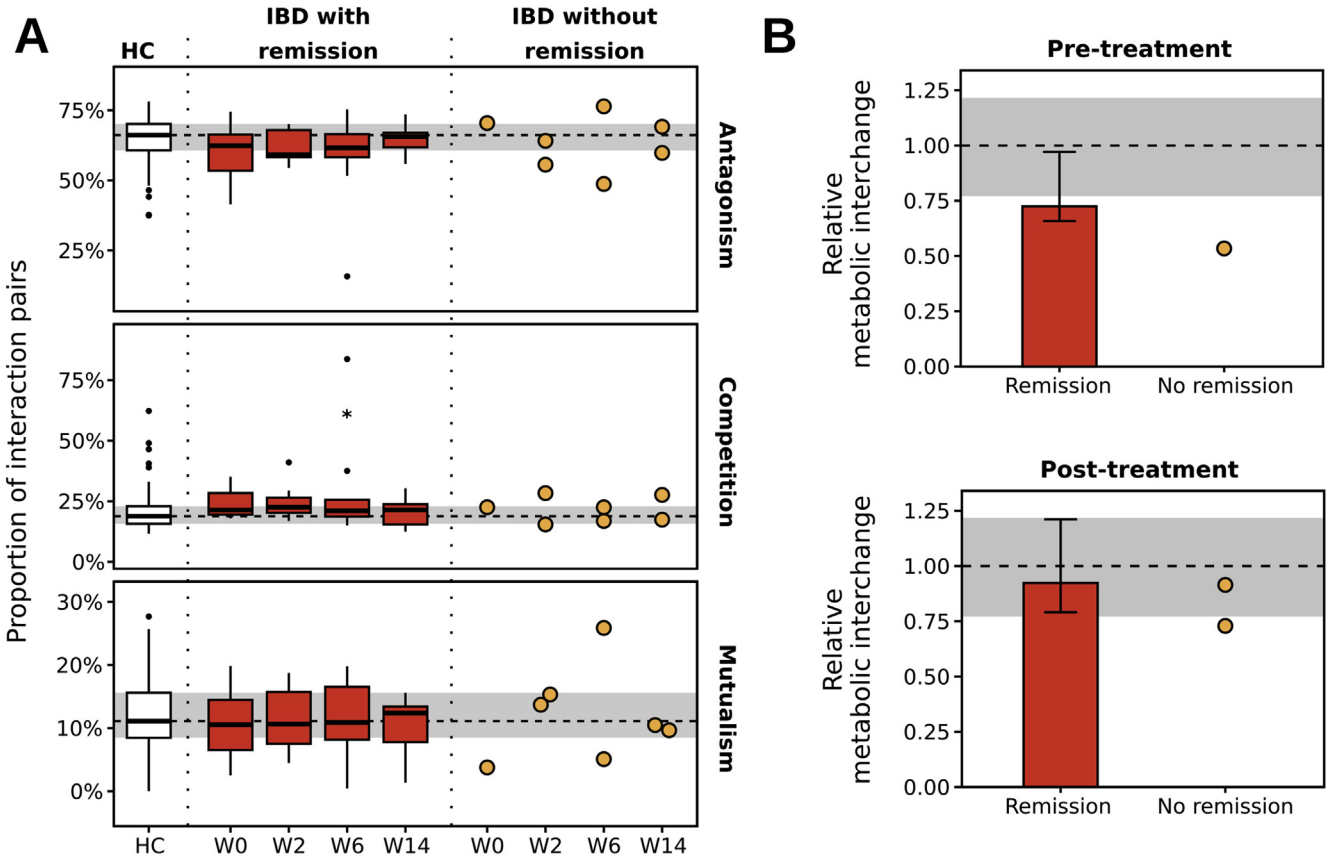

Supplementary Figure 6. In silico–predicted ecological interaction types and total metabolite interchange levels in patients with IBD on anti-$\alpha 4\beta 7$ integrin intervention. (*A*) Fraction of antagonistic (+/−), competitive (−/−), and mutualistic (+/+) interactions among bacterial community members. The dashed line indicates the median value for samples from healthy subjects and the gray area the interquartile range (IQR). (*B*) The predicted total intercellular metabolite fluxes (ie, interchange/cross-feeding) of all metabolites relative to the interchange levels in healthy controls. The dashed line (= 1) indicates the median value and the gray area the IQR for samples from healthy subjects. Bar heights denote the median of predicted interchange estimates for the respective disease group and the patients' remission status. Error bars span the IQR.

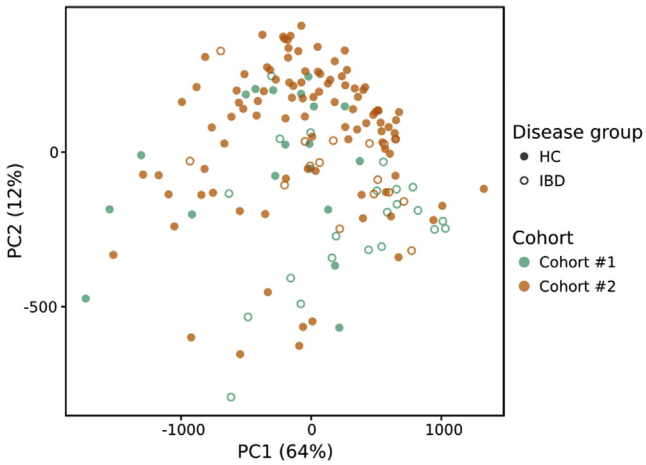

Supplementary Figure 7. Principal component analysis on predicted metabolite exchange rates. Samples from healthy controls and patients with IBD (pretreatment only) and from both cohorts (MAUT and EMED) were combined for this analysis. The analysis included the in silico–predicted cross-feeding rates of 374 different metabolites. Shown are only the first 2 principal component axes, which cover 78% of the observed variability in the data.